Article

Molecular Cell

mHTT Seeding Activity: A Marker of Disease Progression and Neurotoxicity in Models of Huntington's Disease

Graphical Abstract

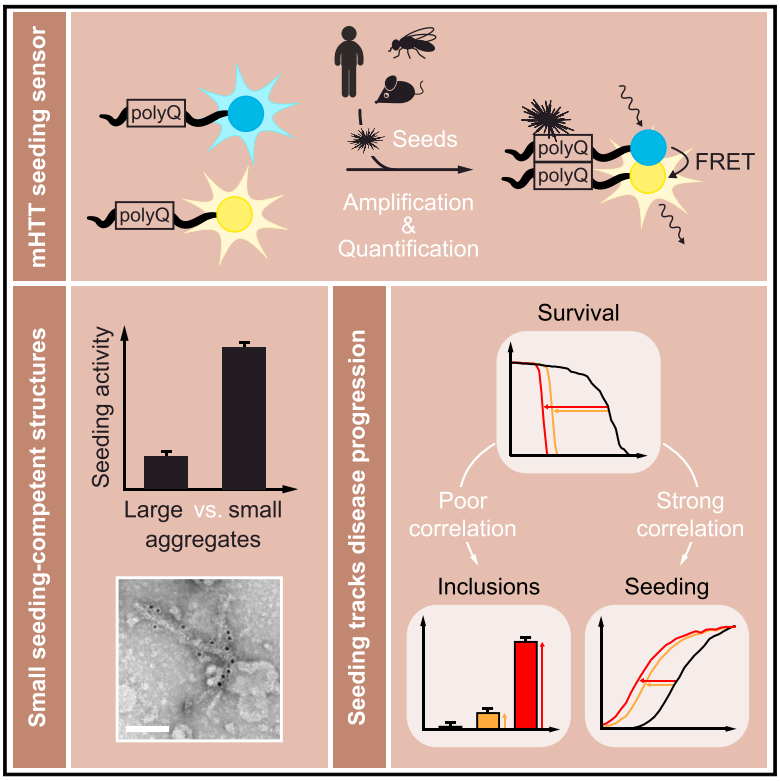

Highlights

- FRASE facilitates quantification of mHTT seeding activity in biosamples
- Small fibrils are likely responsible for mHTT seeding activity in brains of HD mice
- High mHTT seeding activity in neurons correlates with increased mortality in HD flies
- Expression of Hsp70 extends survival and reduces mHTT seeding activity in HD flies

Authors

Anne Ast, Alexander Buntru, Franziska Schindler, ..., Janine Kirstein, Gillian P. Bates, Erich E. Wanker

Correspondence

ewanker@mdc-berlin.de

In Brief

Ast et al. present the development of a FRET-based aggregate seeding (FRASE) assay that facilitates the detection and quantification of mHTT seeding activity (HSA) in complex biosamples. They show that HSA is detectable in brains of presymptomatic Huntington's disease (HD) mice and correlates with disease progression and neurotoxicity in HD transgenic flies.

Ast et al., 2018, Molecular Cell *71*, 675–688
September 6, 2018
https://doi.org/10.1016/j.molcel.2018.07.032

CellPress

Molecular Cell
Article

mHTT Seeding Activity: A Marker of Disease Progression and Neurotoxicity in Models of Huntington's Disease

Anne Ast,[1,2,10] Alexander Buntru,[1,2,10] Franziska Schindler,[1,2,10] Regine Hasenkopf,[1,2] Aline Schulz,[1,2] Lydia Brusendorf,[1,2] Konrad Klockmeier,[1,2] Gerlinde Grelle,[1,2] Benjamin McMahon,[1,2] Hannah Niederlechner,[1,2] Isabelle Jansen,[1,2] Lisa Diez,[1,2] Juliane Edel,[1,2] Annett Boeddrich,[1,2] Sophie A. Franklin,[3] Barbara Baldo,[4] Sigrid Schnoegl,[1,2] Severine Kunz,[5] Bettina Purfürst,[5] Annette Gaertner,[9] Harm H. Kampinga,[6] A. Jennifer Morton,[7] Åsa Petersén,[4] Janine Kirstein,[8] Gillian P. Bates,[3] and Erich E. Wanker[1,2,11,*]

[1]Neuroproteomics, Max Delbrueck Center for Molecular Medicine, 13125 Berlin, Germany
[2]Berlin Institute of Health (BIH), 10178 Berlin, Germany
[3]Huntington's Disease Centre, Department of Neurodegenerative Disease and Dementia Research Institute, UCL Institute of Neurology, London WC1N 3BG, UK
[4]Translational Neuroendocrine Research Unit, Department of Experimental Medical Science, Lund University, 221 84 Lund, Sweden
[5]Electron Microscopy Core Facility, Max Delbrueck Center for Molecular Medicine, 13125 Berlin, Germany
[6]Department of Cell Biology, University Medical Center Groningen, 9713 GZ Groningen, the Netherlands
[7]Department of Physiology, Development and Neuroscience, University of Cambridge, Cambridge CB2 3DY, UK
[8]Proteostasis in Aging and Disease, Leibniz-Institute for Molecular Pharmacology (FMP), 13125 Berlin, Germany
[9]Evotec AG, Manfred Eigen Campus, 22419 Hamburg, Germany
[10]These authors contributed equally
[11]Lead Contact
*Correspondence: ewanker@mdc-berlin.de
https://doi.org/10.1016/j.molcel.2018.07.032

SUMMARY

Self-propagating, amyloidogenic mutant huntingtin (mHTT) aggregates may drive progression of Huntington's disease (HD). Here, we report the development of a FRET-based mHTT aggregate seeding (FRASE) assay that enables the quantification of mHTT seeding activity (HSA) in complex biosamples from HD patients and disease models. Application of the FRASE assay revealed HSA in brain homogenates of presymptomatic HD transgenic and knockin mice and its progressive increase with phenotypic changes, suggesting that HSA quantitatively tracks disease progression. Biochemical investigations of mouse brain homogenates demonstrated that small, rather than large, mHTT structures are responsible for the HSA measured in FRASE assays. Finally, we assessed the neurotoxicity of mHTT seeds in an inducible *Drosophila* model transgenic for *HTTex1*. We found a strong correlation between the HSA measured in adult neurons and the increased mortality of transgenic HD flies, indicating that FRASE assays detect disease-relevant, neurotoxic, mHTT structures with severe phenotypic consequences *in vivo*.

INTRODUCTION

Self-propagating protein aggregates are a pathological hallmark of numerous neurodegenerative diseases (NDs), including Huntington's disease (HD) (Chiti and Dobson, 2017; Jucker and Walker, 2013). Studies indicate that aggregate pathology and associated tissue atrophy do not appear randomly throughout the brain but instead progress along distinct neuronal networks (Brundin et al., 2010). Evidence was provided that amyloidogenic protein assemblies spread from cell to cell, converting free molecules of the same protein into aggregated species. This transcellular propagation may drive pathogenesis in NDs (Guo and Lee, 2014; Pecho-Vrieseling et al., 2014). To understand the mechanisms of disease development and progression, it is of critical importance to specifically monitor the activity of self-propagating protein aggregates in complex biosamples.

Several assays have been established that allow the quantification of seeding activity of amyloidogenic aggregates in crude protein homogenates (Atarashi et al., 2007; Holmes et al., 2014; Tan et al., 2015). These methods take advantage of the phenomenon that ordered protein aggregates are formed from monomers by a nucleation-dependent process (Jarrett and Lansbury, 1993; Scherzinger et al., 1999), a relatively slow process *in vitro*. However, spontaneous amyloid formation can be accelerated by addition of preformed aggregates that function as seeds for the conversion of monomers from a soluble into an aggregated state (Cohen et al., 2012; Jarrett and Lansbury, 1993). Biosamples that contain seeding-competent protein aggregates might therefore stimulate the polymerization of soluble amyloidogenic proteins with related amino acid sequences in cell-free or cell-based seeding assays.

Based on this premise, protein misfolding cyclic amplification (PMCA) technology and related methods (Atarashi et al., 2007, 2011; Saborio et al., 2001) have been developed that allow the detection of minute quantities of seeding-competent PrP^{Sc}

aggregates in various biomaterials prepared from patients or rodent models with prion disease (Castilla et al., 2005). Variants of the PMCA technology have also been applied for the amplification of β-amyloid and α-synuclein aggregates from biosamples (Du et al., 2011; Herva et al., 2014). A key feature of PMCA methods is that seed-mediated amyloid polymerization is indirectly monitored through the reporter dye Thioflavin T (ThT), which changes its fluorescence emission upon binding to ordered amyloid fibrils (Biancalana and Koide, 2010). In addition, cell-based amyloid polymerization assays have been developed (Holmes et al., 2014; Tan et al., 2015). In these assays, ectopically expressed aggregation-prone reporter proteins with fluorescent tags are used as biosensors for detecting amyloidogenic aggregates.

Studies with brain slices and fly and mouse models provide evidence that mutant huntingtin (mHTT) aggregates possess seeding activity and spread from cell to cell (Pecho-Vrieseling et al., 2014; Babcock and Ganetzky, 2015; Pearce et al., 2015), suggesting that proteopathic mHTT seeding in HD patient brains or mouse models drives pathogenesis (Brundin et al., 2010; Jeon et al., 2016). However, it remains unclear whether mHTT seeding is responsible for dysfunction and neurodegeneration. Although several mHTT aggregate species, i.e., small oligomers and fibrils, have been described as potentially pathogenic (Nucifora et al., 2012; Pieri et al., 2012; Scherzinger et al., 1997), the mHTT species that exhibit seeding activity *in vivo* still need to be pinpointed.

To be regarded as disease relevant, we propose that seeding-competent mHTT aggregates need to be detectable in affected brain regions in patients and transgenic HD mouse models. To promote disease development, such structures should be present in model systems before the appearance of a disease phenotype. In addition, their abundance in affected tissues should increase with the severity of disease symptoms. Finally, perturbation of mHTT seeding activity through genetic manipulation should influence the disease phenotype in model systems. In summary, to elucidate the potential importance of mHTT seeding in disease, it is crucial to detect seeding-competent structures in relevant biosamples and to investigate their potential impact on biological functions and phenotypes.

Here, we describe the development of a fluorescence resonance energy transfer (FRET)-based mHTT aggregate seeding (FRASE) assay, which allows the quantification of mHTT seeding activity (HSA) in complex biosamples with high sensitivity and specificity. Application of the method revealed HSA in disease-affected brain tissues of HD patients and mouse models. Furthermore, we observed HSA in brain homogenates of presymptomatic HD mice and its progressive increase with disease development. Biochemical investigations of mouse brain homogenates revealed high HSA predominantly in protein fractions that contain small mHTT fibrils, suggesting that such structures are responsible for this activity *in vivo*. Finally, using an inducible *Drosophila* model of HD, we demonstrated that the formation of seeding-competent huntingtin exon-1 fragment with 97 glutamines (HTTex1Q97) structures in adult neurons is associated with a reduced life span of transgenic flies, indicating that FRASE assays detect neurotoxic structures.

RESULTS

Establishment of a FRET-Based mHTT Aggregate Seeding Assay

To monitor mHTT seeding activity, we first developed a cell-free aggregation assay with recombinant fluorescent reporter proteins (Figure S1A). Two soluble glutathione S-transferase (GST) HTT exon-1 (HTTex1) fusion proteins with 48 glutamines C-terminally fused to CyPet or YPet (GST-Ex1Q48-CyPet or GST-Ex1Q48-YPet) were produced in *E. coli* and purified to ~90% homogeneity using glutathione Sepharose chromatography (Figure S1B).

Recombinant proteins were cleaved with PreScission protease (PSP) to release GST and to initiate the spontaneous aggregation of the fusion proteins Ex1Q48-CyPet and Ex1Q48-YPet. The assembly of the tagged Ex1Q48 proteins into insoluble aggregates over time was monitored using an established filter retardation assay (FRA), which specifically detects large SDS-stable mHTT aggregates (Wanker et al., 1999). We found that the proteins Ex1Q48-CyPet and Ex1Q48-YPet rapidly self-assemble into SDS-stable aggregates *in vitro* (Figure 1A), confirming reported results (Wagner et al., 2018). To investigate the morphology of spontaneously formed Ex1Q48-CyPet and Ex1Q48-YPet aggregates, we analyzed the aggregation reactions with atomic force microscopy (AFM). We observed that the tagged Ex1Q48 fusion proteins, similar to the untagged Ex1Q48 protein (Wagner et al., 2018), form large fibrillar protein aggregates (Figure 1B).

We hypothesized that co-aggregation of CyPet- and YPet-tagged HTTex1 fragments should lead to a time-dependent increase of FRET as the fluorescent tags are brought close when fibrillar aggregates are formed (Figure 1C). We treated mixtures of fusion proteins (1:1 molar ratio; 1–3 μM concentrations) with PSP and quantified the spontaneous formation of Ex1Q48-CyPet/-YPet co-aggregates by repeated FRET measurements. We observed a time- and concentration-dependent increase of FRET efficiency (Figure 1D), indicating that FRET measurements are suitable to quantify HTTex1 co-aggregation. In contrast, no time-dependent increase of FRET efficiency was observed in samples that were not treated with PSP, underlining that the removal of the GST tag from CyPet- and YPet-tagged Ex1Q48 fragments is critical for the self-assembly of co-aggregates. Proteolytic cleavage of the GST fusion proteins with PSP was confirmed by SDS-PAGE and immunoblotting (Figure S1C). Finally, AFM analysis confirmed that the samples contain typical fibrillar HTTex1 co-aggregates (Figure S1D).

To assess whether preformed Ex1Q48 fibrils can seed the co-aggregation of Ex1Q48-CyPet/-YPet, we incubated a 1:1 mixture of the GST fusion proteins with PSP and different amounts of preformed Ex1Q48 fibrils as seeds. We observed that addition of fibrils shortens the lag phase of Ex1Q48-CyPet/-YPet polymerization in a concentration-dependent manner (Figure 1E), indicating that they possess seeding activity. We termed the established method, which permits the quantification of mHTT seeding activity (HSA) in samples of interest, FRET-based mHTT aggregate seeding (FRASE) assay.

In independent control experiments, we also investigated whether a mixture of fusion proteins with non-pathogenic

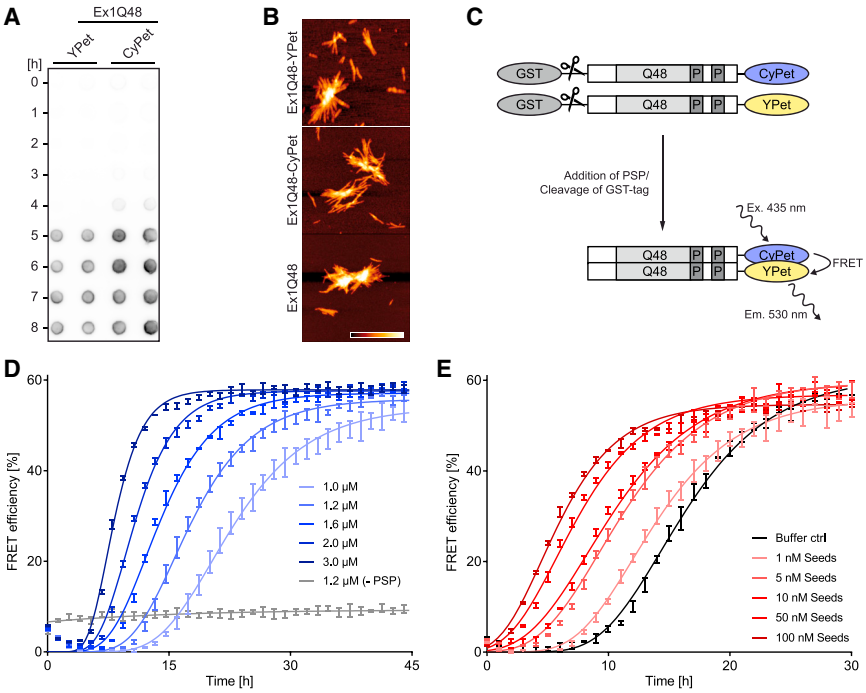

Figure 1. Establishment of a FRET-Based mHTT Aggregate Seeding Assay

(A) Time-dependent aggregation of Ex1Q48-CyPet and Ex1Q48-YPet fusion proteins (3 μM) monitored by FRA (500 ng protein per dot). Immunoblot, anti-GFP antibody.

(B) Analysis of spontaneously formed Ex1Q48-CyPet, Ex1Q48-YPet, and Ex1Q48 aggregates by AFM (3 μM) after 24 hr. Scale bars: 1 μm. Color gradient represents a 0 to 20 nm height.

(C) Schematic model of FRET-inducing co-aggregating Ex1Q48-CyPet and Ex1Q48-YPet upon cleavage of GST fusion proteins with PSP.

(D) Spontaneous time-dependent co-aggregation of Ex1Q48-CyPet and Ex1Q48-YPet sensor proteins (1:1 mixture) upon incubation of GST fusion proteins with PSP at 25°C. FRET efficiency is displayed as mean ± SD of technical triplicates.

(E) Fibrillar Ex1Q48 aggregates (seeds) induce a concentration-dependent shortening of the lag phase in Ex1Q48-CyPet and Ex1Q48-YPet (1:1 mixture, 1.2 μM) co-polymerization reactions. Seed concentrations are equivalent to monomer concentrations. FRET efficiency is displayed as mean ± SD of technical triplicates.

See also Figure S1.

polyglutamine (polyQ) tracts, GST-Ex1Q23-CyPet/-YPet (Figure S1A), can be applied as reporter molecules to monitor HSA. We found that preformed, fibrillar Ex1Q48 seeds do not induce FRET when they are added to PSP-treated GST-Ex1Q23-CyPet/-YPet fusion proteins (Figure S1E). Finally, we confirmed that addition of proteolytically cleaved GST-Ex1Q23 fusion protein, as well as of uncleaved GST-Ex1Q23 or GST-Ex1Q48 fusion proteins, does not shorten the lag phase of Ex1Q48-CyPet/-YPet polymerization (Figure S1F).

Both Small and Large Ex1Q48 Fibrils Exhibit HSA in FRASE Assays

Our initial experiments indicate that large bundles of Ex1Q48 fibrils (~1–2 μm in length) (Figure 1B) possess HSA (Figure 1E). We next investigated whether such an activity can also be detected when small fibrillar Ex1Q48 seeds are added to FRASE assays. We sonicated large preformed Ex1Q48 fibrils for different periods and subsequently determined the HSA. We found that seeding activity is high in sonicated Ex1Q48 preparations (Figures S2A and S2B), indicating that small, not just large, Ex1Q48 fibrils possess HSA. To confirm that small fibrils are produced, we analyzed the generated samples by FRA (Wanker et al., 1999). We detected large Ex1Q48 aggregates in non-sonicated samples (Figure S2C), whereas they were not observed in sonicated samples (>30 s). This indicates that sonication (>30 s) leads to fibril breakage and the formation of small HTTex1 structures that are no longer retained on filter membranes. Next, the samples were analyzed by dot blot (DB) assays, which allow the identification of protein assemblies on filter membranes independent of their size (Kayed et al., 2003). These experiments revealed Ex1Q48 immunoreactivity in both sonicated and non-sonicated samples (Figure S2C), confirming the presence of mHTTex1 protein in all samples. Finally, we analyzed the generated samples with AFM, indicating that small fibrillar Ex1Q48 structures are produced by sonication (Figure S2D).

FRASE Assays Detect HSA with High Sensitivity and Specificity

To investigate the sensitivity and specificity of FRASE assays, we generated recombinant Ex1Q48 seeds by sonication and analyzed them using blue native PAGE and immunoblotting. We found that sonication for 60 s leads to the formation of Ex1Q48 structures with an average molecular weight of ~1,250 kDa (~90-mers) (Figure 2A), whereas larger aggregates were detected in non-sonicated samples.

Next, a large range of concentrations of sonicated Ex1Q48 seeds was analyzed for their activity in FRASE assays. As expected, we observed a dose-dependent shortening of the lag phase when Ex1Q48 structures were added to polymerization reactions (Figures 2B and 2C). We determined a threshold of ~60 fM for detecting Ex1Q48 seeds. Furthermore, FRASE assays responded quantitatively to seeds over a dynamic range of 4 orders of magnitude (Figure 2C). At a concentration of ~560 fM, the Z′ factor (Zhang et al., 1999) was 0.67 (Figure 2C).

Finally, we investigated the specificity of the FRASE assay for detecting mHTTex1 aggregates. We produced fibrillar α-synuclein, tau, β-amyloid, and islet amyloid polypeptide (IAPP) aggregates *in vitro* and subsequently analyzed them in FRASE assays. The unrelated fibrillar aggregates did not significantly influence Ex1Q48-CyPet/-YPet polymerization (Figure 2D), indicating that the FRASE assay specifically detects amyloidogenic mHTTex1 aggregates. AFM analysis confirmed that fibrillar α-synuclein, tau, β-amyloid, and IAPP aggregates were added to reactions (Figure 2E).

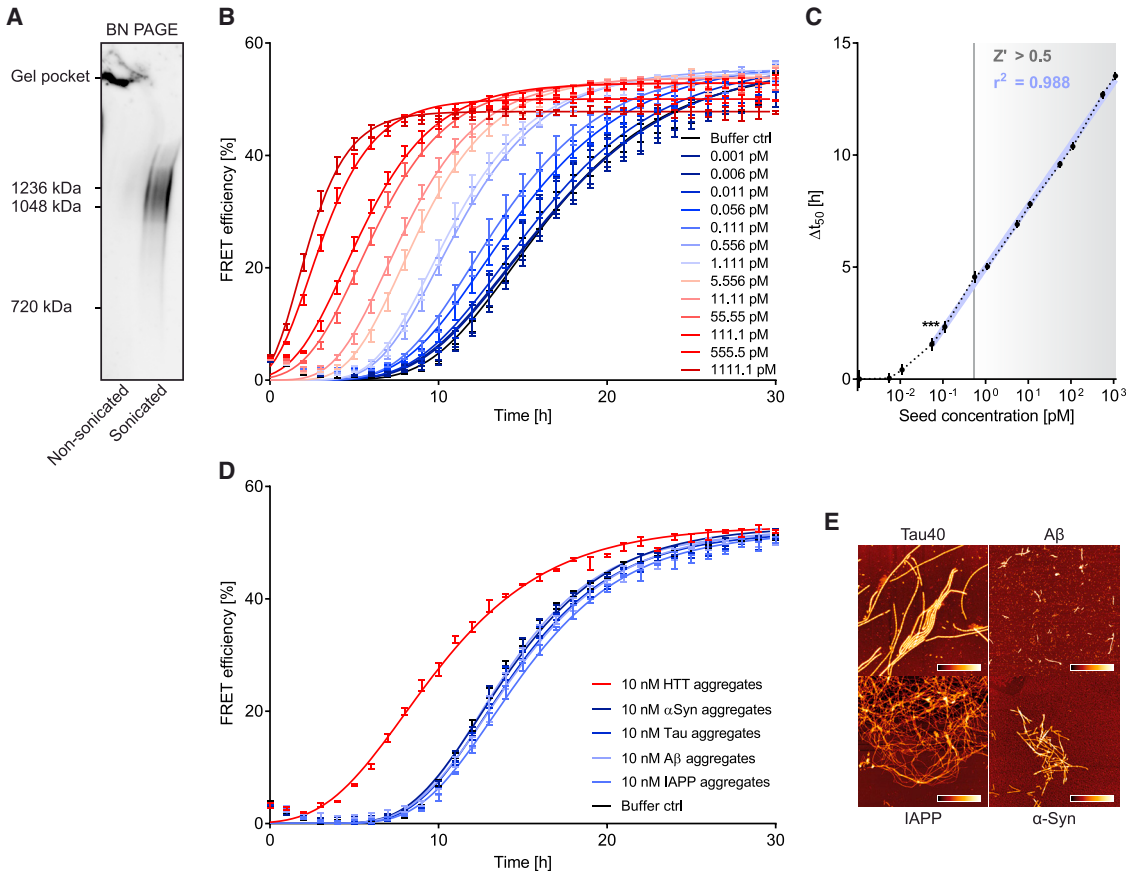

Figure 2. FRASE Assays Facilitate Detection of HSA with High Specificity and Sensitivity

(A) Analysis of sonicated (1 min) and non-sonicated fibrillar Ex1Q48 aggregates by blue native (BN) PAGE and immunoblotting using HD1 antibody.

(B) Effects of small, preformed Ex1Q48 seeds (~1,250 kDa) on Ex1Q48-CyPet and Ex1Q48-YPet (1:1 mixture, 1.2 μM) co-aggregation. Data are mean ± SEM (n = 5).

(C) Calculation of HSAs (Δt_{50} values) from aggregation profiles in (B). Data are mean ± SEM (n = 5).

(D) Effects of non-polyQ fibrils on Ex1Q48-CyPet and Ex1Q48-YPet (1:1 mixture, 1.2 μM) co-aggregation. Data are mean ± SD of triplicates.

(E) Analysis of α-synuclein (α-Syn), β-amyloid 42 (Aβ), islet amyloid polypeptide (IAPP), and tau (Tau40) fibrils by AFM. Scale bars: 1 μm. Height of color gradients: 0–10 nm (α-Syn), 0–5 nm (Aβ), 0–30 nm (IAPP), and 0–10 nm (Tau40).

See also Figure S2.

HSA Is Detectable in Brains of HD Mice and Patients

To investigate whether FRASE assays detect HSA in complex biosamples (Figure 3A), we first assessed brain homogenates prepared from 12-week-old R6/2Q212 transgenic mice (carrying ~212 CAGs) and age-matched controls. R6/2Q212 mice express low levels of the human HTTex1Q212 protein (Sathasivam et al., 2013) and show motor abnormalities from 8 weeks of age (Carter et al., 1999) and typical mHTTex1 inclusion bodies from 3 or 4 weeks onward (Li et al., 1999). We detected high levels of HSA in brain homogenates of R6/2Q212 mice, but not in those of age-matched littermate controls (Figures 3B and 3C), indicating the presence of seeding-competent mHTTex1 structures. Independent control experiments with the non-pathogenic reporter molecules Ex1Q23-CyPet/-YPet did not reveal detectable HSA in R6/2Q212 brain homogenates (Figure S3A).

Next, we assessed whether HSA is detectable in brain extracts of 12-week-old R6/2Q51 mice (Larson et al., 2015), which express a HTTex1Q51 fragment. In comparison to R6/2Q212 mice, these mice do not yet have a disease phenotype at 12 weeks of age, suggesting that HSA should be lower. FRASE analysis revealed that brain homogenates of prodromal 12-week-old R6/2Q51 mice do not possess significant HSA (Figure S3B), although activity was detectable in extracts of old mice (104–105 weeks), which show pathological signs of disease.

We also investigated whether HSA is detectable in the hypothalamus of mouse brains, in which the proteins HTT853-Q79 or HTT853-Q18 were overexpressed for 8 weeks using viral vectors. Previous studies have demonstrated that hypothalamic expression of HTT853-Q79 leads to a gain of body weight and the formation of insoluble mHTT protein aggregates (Hult et al., 2011). We found that HTT853-Q79 mice were significantly heavier than control and HTT853-Q18 mice (Figure S3C). We also observed significantly higher HSA in brain homogenates of HTT853-Q79 mice compared to HTT853-Q18 and control mice (Figure S3D), indicating that seeding activity and alterations in body weight are associated.

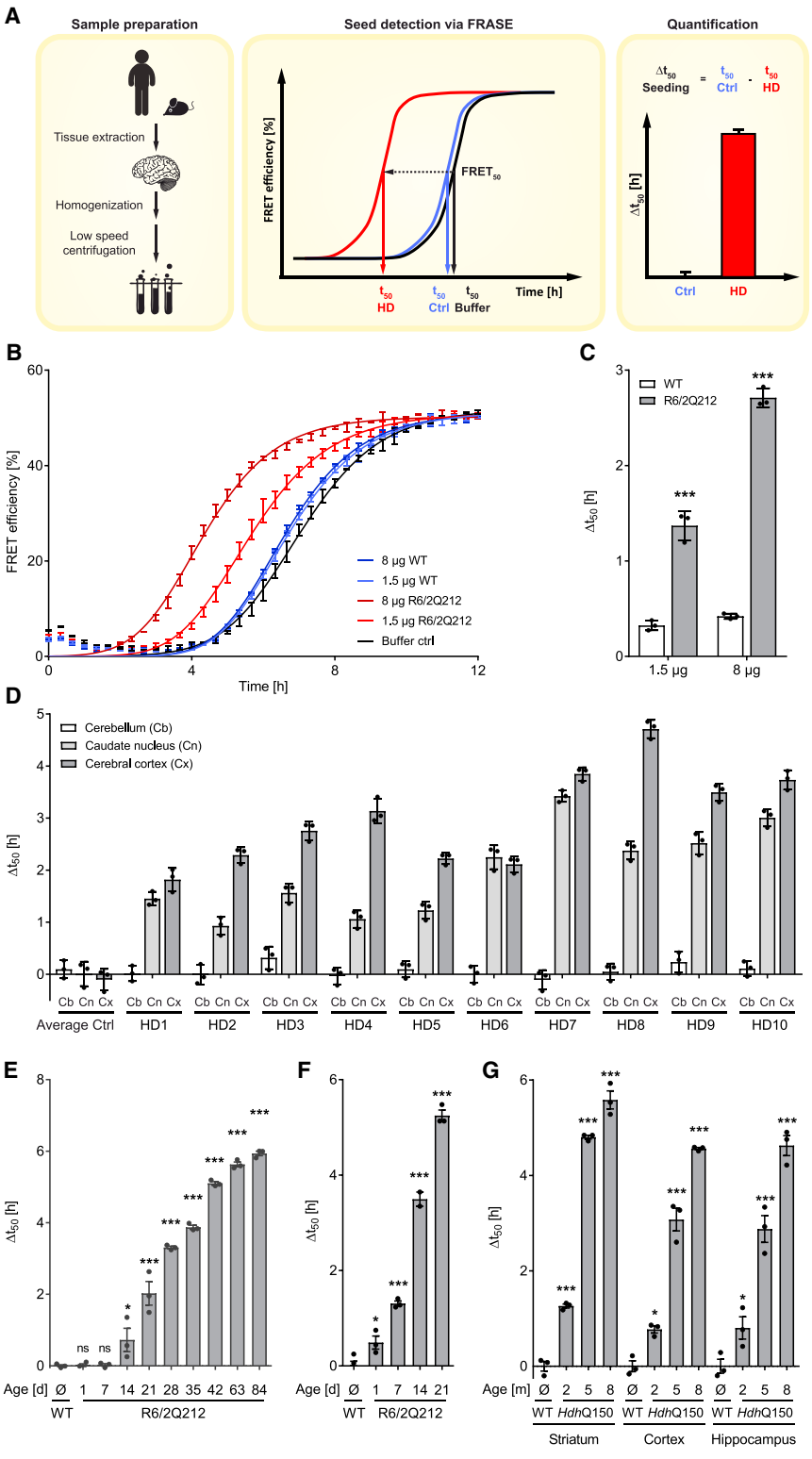

Figure 3. Quantification of HSA in Brain Extracts of Patients and HD Mice

(A) Schematic workflow for quantifying HSA in brain tissue homogenates.

(B) Effects of mouse brain homogenates on Ex1Q48-CyPet and Ex1Q48-YPet (1:1 mixture, 3 µM) co-aggregation. Data are mean ± SD of technical triplicates.

(C) HSA (Δt_{50} values) of mouse brain extracts investigated in (B). Statistical analysis: two-way ANOVA followed by Bonferroni's multiple comparison post hoc test against the respective wild-type (WT) controls. Δt_{50} is displayed as individual values (•) and as mean ± SD of technical triplicates.

(D) Quantification of HSA in brain homogenates prepared from HD patients and controls. For clarity, the average Δt_{50} values obtained from three healthy control samples are depicted (Average Ctrl). Individual values of Δt_{50} (•) and mean ± SD of triplicates are displayed.

(E) Quantification of HSA in brain extracts of R6/2Q212 and WT control mice (3 mice per age). Results from WT mice are shown as an average Δt_{50} value.

(F) Quantification of HSA in brain extracts of pre-symptomatic R6/2Q212 and WT control mice after sonication. Results from WT mice are shown as an average Δt_{50} value.

(G) Quantification of HSA in brain tissue extracts of *Hdh*Q150 heterozygous knockin and WT mice. Data are mean ± SEM (n = 3). One-way ANOVA followed by Dunnett's multiple comparison test. See also Figure S3.

We next examined HSA in brain regions of HD patients. Protein extracts prepared from postmortem tissue (cerebral cortex, caudate nucleus, and cerebellum) from HD patients and control individuals were systematically analyzed using the FRASE assay. HSA was invariably detected in HD patients, but not in control samples (Figure 3D), indicating that the method is suitable to discriminate between patients and healthy individuals. HSA was detectable in the cerebral cortex and the caudate nucleus, which are severely affected in HD patients (Zuccato et al., 2010), but it was not observed in the cerebellum, which is less affected in disease (DiFiglia et al., 1997). Similarly, no HSA was detectable in postmortem brains of patients with Alzheimer's disease (AD) that do not contain abnormal polyQ aggregates (Figure S3E).

Finally, we investigated whether HSA in biosamples originates from mHTT seeds. We produced brain extracts from symptomatic 12-week-old R6/2Q212 mice and littermate controls and immunodepleted potential seeding-competent mHTTex1 seeds using the monoclonal anti-HTT antibody MW8 (Ko et al., 2001). Then, samples were analyzed using FRASE assays. We observed a dramatic decrease of HSA in MW8-immunodepleted R6/2Q212 brain homogenates, but not

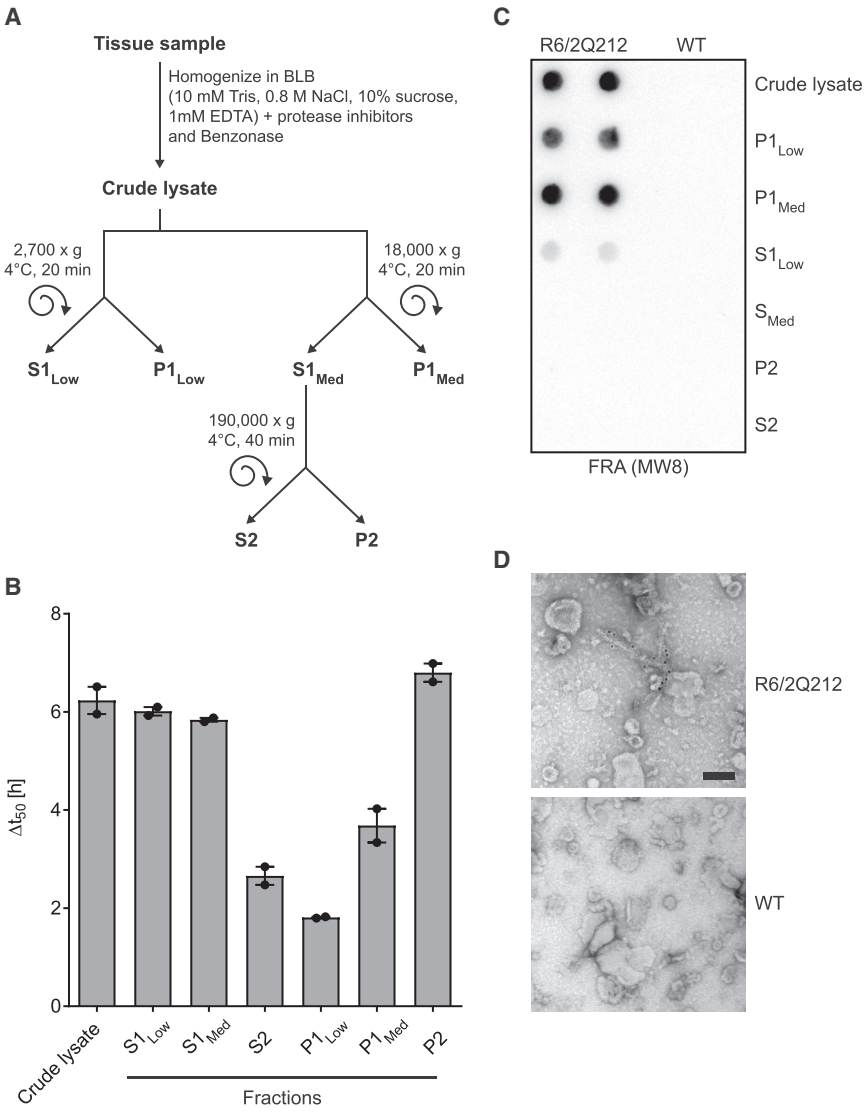

Figure 4. Detection of Small HTTex1 Fibrils in Soluble Brain Fractions with High HSA

(A) Schematic workflow for preparing soluble and insoluble protein fractions from crude tissue homogenates by centrifugation.

(B) Quantification of HSA in soluble and insoluble fractions prepared from brains of R6/2Q212 transgenic mice. In all cases, data were normalized to average Δt_{50} values of age-matched WT control mice. Error bars are mean ± SEM (n = 2). HSAs measured for individual mice are displayed as dots (•).

(C) Detection of large, SDS-stable fibrillar mHTTex1 aggregates in protein fractions by FRA.

(D) Detection of small, fibrillar HTTex1 aggregates in P2 fractions of R6/2Q212 mice by immunoelectron microscopy using the anti-HTT antibody Agg53. Scale bar: 100 nm.

in homogenates treated with an isotype control antibody (Figures S3F and S3G), indicating that antibody treatment removes seeding-competent mHTTex1 aggregates from mouse brain extracts. As expected, we did not detect HSA in crude brain extracts of age-matched wild-type control mice. SDS-PAGE and immunoblotting confirmed depletion of mHTTex1 protein aggregates from brain homogenates by MW8 antibody treatment (Figures S3H and S3I).

FRASE Assay Detects HSA in Brains of Presymptomatic HD Mice

To address whether HSA is detectable in brains of presymptomatic HD mice, we first analyzed non-sonicated brain homogenates of young R6/2Q212 mice and age-matched controls using the FRASE assay. We detected significant HSA in brain extracts of 2-week-old R6/2Q212 mice (Figure 3E) that progressively increased over time. A similar result was obtained with sonicated brain extracts (Figure 3F). With sonication, significant HSA was already detectable in brains of 1-day-old R6/2Q212 transgenic mice, indicating that seeding-competent mHTTex1 structures are present in brains of R6/2Q212 mice long before inclusion bodies or motor abnormities can be detected (Davies et al., 1997; Zuccato et al., 2010).

Next, we investigated whether HSA is detectable in presymptomatic *Hdh*Q150 knockin mice that express a full-length mHTT protein with a pathogenic polyQ tract of 150 glutamines (Lin et al., 2001). These mice show onset of depressive-like symptoms by 12 months of age (Ciamei et al., 2015) and impairment of motor function ~18 months of age. Widespread deposition of mHTT aggregates throughout the brain is observed by 8 months of age (Woodman et al., 2007). We systematically analyzed tissue homogenates prepared from cortex, striatum, and hippocampus of 2-, 5-, and 8-month-old heterozygous *Hdh*Q150 mice and littermate controls using the FRASE assay. We observed progressively increasing HSA in protein extracts from all three brain regions of *Hdh*Q150, but not from control mice (Figure 3G), confirming that mHTT seeds are detectable in HD mouse brains long before the appearance of inclusion bodies and motor abnormalities (Woodman et al., 2007).

HSA Is Detectable in Protein Fractions after Depletion of Large mHTTex1 Aggregates by Centrifugation

To investigate whether HSA in HD mouse brains originates predominantly from soluble or insoluble mHTTex1 aggregates, non-sonicated brain homogenates prepared from symptomatic 12-week-old R6/2Q212 mice were centrifuged for 20 min at 2,700 × *g* (low speed) or 18,000 × *g* (medium speed), respectively, and the resulting supernatant and pellet fractions ($S1_{Low}$ and $P1_{Low}$ or $S1_{Med}$ and $P1_{Med}$) (Figure 4A) were analyzed with FRASE assays. HSA was high in the parental crude lysate and

in the $S1_{Low}$ fraction, while it was relatively low in the $P1_{Low}$ fraction (Figure 4B), suggesting that it predominantly originates from soluble, rather than insoluble, mHTTex1 aggregates. A similar result was obtained when the fractions $S1_{Med}$ and $P1_{Med}$ were analyzed (Figure 4B). However, after medium-speed centrifugation, HSA in the $P1_{Med}$ fraction was higher than in the $P1_{Low}$ fraction, indicating that mHTTex1 seeds can be removed from supernatant fractions using a higher centrifugation speed. This trend was even more pronounced when the generated $S1_{Med}$ fraction was subjected to high-speed centrifugation (190,000 × *g*), resulting in the supernatant and pellet fractions S2 and P2 (Figure 4A). FRASE analysis revealed significantly higher HSA in the P2 than in the S2 fraction, indicating that small seeding-competent mHTTex1 aggregates can be removed from the soluble $S1_{Med}$ fraction by high-speed centrifugation (Figures 4A and 4B).

To obtain a first hint about the size of the seeding-competent mHTTex1 aggregates in the brains of R6/2Q212 mice, the supernatant and pellet fractions were analyzed by FRA (Wanker et al., 1999). We found mHTTex1 immunoreactivity predominantly in the $P1_{Low}$ and $P1_{Med}$ fractions. In comparison, weak or no immunoreactivity was detected in the fractions $S1_{Low}$, $S1_{Med}$, P2, and S2 (Figure 4C), suggesting that HSA in R6/2Q212 mouse brain extracts predominately originates from small, rather than large, mHTTex1 protein assemblies.

Finally, we used transmission immunoelectron microscopy to assess the size and morphology of mHTTex1 seeds present in P2 fractions. They exhibit high HSA but do not contain large mHTTex1 aggregates. We detected small, immunoreactive mHTTex1 fibrils with diameters of 10.2 ± 3.6 nm and lengths of 157.8 ± 64.1 nm exclusively in P2 fractions of R6/2Q212 mice (Figure 4D), suggesting that HSA originates from such structures in P2 fractions.

Establishment of an Inducible HD *Drosophila* Model

To elucidate whether mHTTex1 seeds are disease-relevant structures that cause dysfunction and toxicity in neurons, it is necessary to investigate their phenotypic consequences *in vivo* in the absence of large insoluble aggregates and without continuous overproduction of mHTT protein. We hypothesized that short-term production of small amounts of mHTTex1 seeds in adult neurons might be sufficient to cause neurotoxicity in HD flies.

Using the bacteriophage ΦC31 integration system, cDNAs encoding HTTex1 proteins with normal and pathogenic polyQ tracts (HTTex1Q17 and HTTex1Q97) were integrated into an intergenic locus (Bischof et al., 2007). Genotypes of newly created strains were confirmed by PCR using genomic DNA (Figure S4A). To investigate whether the generated fly strains are comparable regarding their life span, we generated the fly lines w1118;HTTex1Q17 and w1118;HTTex1Q97 that carry the transgenes but lack the GAL4 driver, which is required for transgene expression. Measuring fly survival revealed a median life span of ~102 days for both strains (Figure S4B).

To induce HTTex1 protein expression in adult neurons, we used the inducible, pan-neuronal Elav-GeneSwitch (elavGS) driver (Figure S4C). This driver (Osterwalder et al., 2001) was applied previously to create adult-onset *Drosophila* models for spinocerebellar ataxia 7 (Latouche et al., 2007), suggesting that it may also be suitable to temporarily produce polyQ-containing HTTex1 proteins in neurons. Transgene expression in neurons of elavGS flies is induced when they are supplied with food containing the hormonal inducer RU486. Transgene expression can be switched off when flies are transferred back to food lacking the inducer (Rogers et al., 2012).

We first investigated whether RU486 treatment induces transgene expression in elavGS;HTTex1Q97 flies. We incubated adult flies for 1, 3, 6, and 12 days on food containing RU486 (400 μM) and quantified HTTex1Q97 transcript levels in fly heads by qPCR. We measured high amounts of HTTex1Q97 transcripts in brains of RU486-treated flies, but not untreated flies (Figures S4D and S4E), confirming the functionality of the expression system. Similar results were obtained when elavGS;HTTex1Q17 flies were analyzed (data not shown).

Finally, we assessed whether large mHTTex1 aggregates and/or HSAs are detectable in brains of RU486-treated elavGS HD flies. Starting at an age of 3 days, we treated elavGS;HTTex1Q97 and elavGS;HTTex1Q17 flies for 24 days with the hormone RU486. Head lysates were prepared and subsequently analyzed by FRA and FRASE assays. We observed the formation of large SDS-stable aggregates by FRA in head extracts of RU486-treated elavGS;HTTex1Q97 flies (Figure S4F). Such structures, however, were undetectable in untreated elavGS;HTTex1Q97 flies. Similarly, no SDS-stable aggregates were detectable in RU486-treated and untreated elavGS; HTTex1Q17, w1118;HTTex1Q17, and w1118;HTTex1Q97 flies (Figure S4F). In head lysates of hormone-treated elavGS; HTTex1Q97 flies, HSA was also detectable by FRASE assays (Figure S4G). It was undetectable in brains of untreated elavGS;HTTex1Q97 flies, as well as in treated and untreated elavGS;HTTex1Q17, w1118;HTTex1Q17, and w1118; HTTex1Q97 flies of the same age (Figure S4G).

Short-Term Expression of HTTex1Q97 in Adult Neurons Decreases Life Span and Locomotor Activity of HD Flies

We first confirmed that HTTex1 transcripts decline in neurons when HTTex1Q97-expressing elavGS;HTTex1Q97 flies are placed back on food without the inducer (Figures S5A and S5B). Next, we investigated whether both long- and short-term expression of HTTex1Q17 or HTTex1Q97 in adult neurons influences survival of HD flies. Starting at an age of 3 days, we treated elavGS;HTTex1Q17 and elavGS;HTTex1Q97 flies either continuously or only for a short time of 3 or 6 days with RU486 (Figure 5A); survival was measured by counting dead flies. We found that the life span of chronically RU486-treated elavGS;HTTex1Q97 flies was significantly reduced in comparison to untreated flies (Figures 5B and 5C). In contrast, chronic treatment with RU486 did not shorten the life span of elavGS;HTTex1Q17 flies. We calculated a median life span of ~30 and ~85 days for treated and untreated elavGS; HTTex1Q97 flies, respectively. Median life spans (~38 and ~33 days) of short-term and chronically treated elavGS; HTTex1Q97 flies were similar.

As a behavioral measure of neuronal dysfunction, locomotor activity of HD flies was assessed using a negative geotaxis (climbing) assay (Latouche et al., 2007). We observed that RU486-treated elavGS;HTTex1Q97 flies show a significant

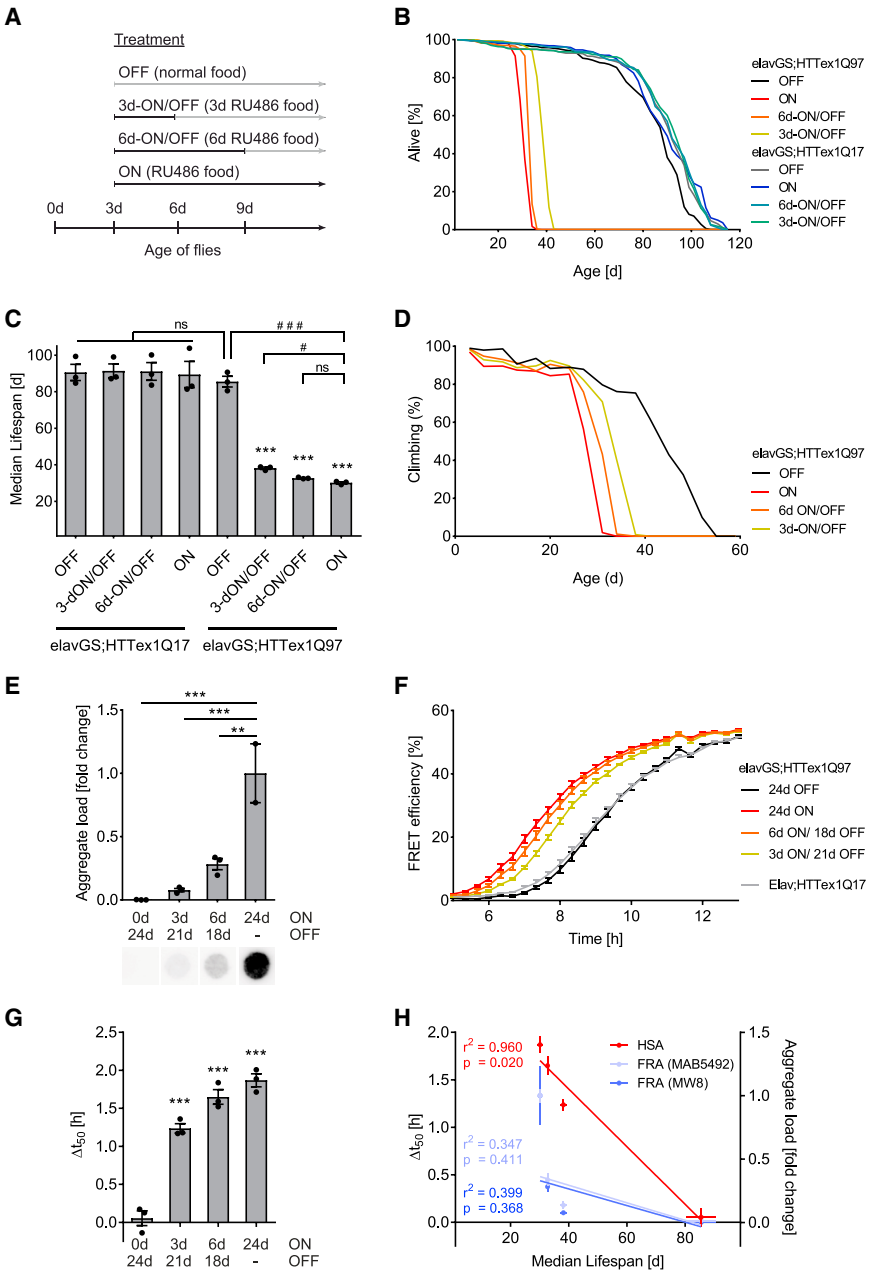

Figure 5. Short-Term HTTex1Q97 Expression-Induced Decrease in *Drosophila* Life Span Correlates with HSA, but Not with Aggregate Load in General

(A) Scheme for short- and long-term RU486 treatment of adult HD transgenic flies.

(B) Survival of RU486-treated and untreated elavGS;HTTex1Q97 and elavGS;HTTex1Q17 flies (n = ~100 flies/group). Survival was plotted as the percentage of surviving flies of three biological replicates.

(C) Median life span calculated from survival curves in (B). Average survival of each experiment (n = ~100 flies/group) is presented as dots (•). Error bars are mean ± SEM from three independent experiments. One-way ANOVA followed by Dunnett's post hoc test. NS, not statistically significant; */# $p < 0.05$; **/## $p < 0.01$; ***/### $p < 0.001$.

(D) Analysis of motor performance of RU486-treated and untreated elavGS;HTTex1Q97 flies (n = ~100 flies/group; three independent experiments).

(E) Quantification of large, SDS-stable fibrillar HTTex1 aggregates in heads of RU486-treated and untreated elavGS;HTTex1Q97 flies by FRA using the MW8 antibody. Representative images for each condition are shown. Data are mean ± SEM of individual measurements (•). One-way ANOVA followed by Dunnett's post hoc test.

(F) FRASE analysis of head lysates analyzed in (E). Values are means ± SEM of three biological replicates each performed in triplicate.

(G) Quantification of HSA (Δt_{50} values) from FRET-based aggregation profiles depicted in (F). Results are displayed as mean ± SEM; individual measurements are presented as dots (•). One-way ANOVA followed by Dunnett's post hoc test.

(H) Pearson correlation analysis. Data are mean ± SEM of the three independent experiments.

See also Figures S4 and S5.

decline in climbing behavior in comparison to untreated controls (Figure 5D), confirming that both short- and long-term expression of HTTex1Q97 in adult neurons induces neurotoxicity in HD flies.

Formation of Small, Seeding-Competent HTTex1Q97 Structures in Adult Neurons Is Associated with Reduced Survival

We first assessed the correlation between the formation of large, SDS-stable HTTex1 aggregates in neurons and the survival of RU486-treated elavGS;HTTex1Q97 flies (Figures 5B and 5C). Head lysates were prepared from continuously and short-term (3 and 6 days) RU486-treated and untreated flies (Figure S5C) and analyzed by FRA using the anti-HTT antibody MW8 (Ko et al., 2001). We found that the abundance of large, SDS-stable HTTex1Q97 aggregates was high in heads of chronically RU486-treated elavGS;HTTex1Q97 flies but relatively low in short-term treated flies (Figure 5E). A similar result was obtained when the formation of large HTTex1Q97 aggregates in fly heads was quantified by FRAs using the anti-HTT antibody MAB5492 (Figure S5D). These results indicate that large HTTex1Q97 aggregates detected by FRAs in adult neurons cannot predict the observed survival phenotypes, which are similar for short- and long-term RU486-treated flies (Figures 5B and 5C).

We next investigated mHTTex1 aggregate formation in brains of hormone-treated elavGS;HTTex1Q97 flies using an immunohistochemical method. We dissected whole brains of short- and long-term treated elavGS;HTTex1Q97 flies (Figure S5C) and incubated them with the antibody MAB5492. As

a control, the brain sections were also immunoassayed with an anti-RBP (RIM-binding protein) antibody, which detects synapses (Liu et al., 2011). As expected, we detected high numbers of HTTex1Q97 aggregates (green puncta) in long-term and lower numbers in short-term (3 and 6 days) hormone-treated HD flies (Figure S5E), confirming the results obtained by FRAs (Figure 5E). These investigations also revealed very low numbers of HTTex1Q97 aggregates in brains of non-induced elavGS;HTTex1Q97 flies (Figure S5E), indicating that the elavGS expression system is leaky and very low levels of HTTex1Q97 protein are also produced in the absence of hormone treatment. However, such a low expression of HTTex1Q97 was not sufficient to significantly shorten the life span of HD flies (Figure 5C).

Finally, we used the FRASE assay to quantify HSA in head lysates of RU486-treated elavGS;HTTex1Q97 flies. We measured high HSA in protein lysates of both short- and long-term hormone-treated flies (Figures 5F and 5G), demonstrating that FRASE assays provide information that is fundamentally different from that obtained by FRAs. Because the abundance of large fibrillar aggregates is very low in protein extracts of short-term treated flies (Figures 5E and S5D), HSA in these fractions must predominantly result from small structures that are not retained by the filter membrane. In contrast to the FRA results (Figures 5E and S5D), HSA levels measured with the FRASE assay (Figures 5F and 5G) correlate significantly better with the increased mortality of RU486-treated elavGS;HTTex1Q97 flies (Figure 5H). As expected, HSA was undetectable in head lysates of 27-day-old elav;HTTex1Q17 control flies, which constitutively express the protein HTTex1Q17 in neurons (Figure 5F).

Short-Term Expression of Hsp70 Extends the Life Span of HD Flies and Decreases HSA in Neurons

We hypothesized that co-expression of the molecular chaperone heat shock protein 70 (Hsp70) (*HSPA1L*) (Chan et al., 2000) might influence HSA and neurotoxicity in HD transgenic flies. To address this question, we generated elavGS;HSPA1L;HTTex1Q97 flies, which upon hormone treatment co-produce both Hsp70 and HTTex1Q97 in adult neurons. We first assessed whether similar levels of HTTex1Q97 transcripts are expressed in brains of RU486-treated elavGS;HSPA1L;HTTex1Q97 and elavGS;HTTex1Q97 flies. We treated 3-day-old flies for 6 days with RU486 (400 μM) and subsequently quantified mHTTex1 transcript levels in fly heads by qPCR. Similar HTTex1Q97 transcript levels were observed in both strains, indicating that co-expression of *HSPA1L* does not significantly influence mHTTex1 expression in elavGS;HSPA1L;HTTex1Q97 flies (Figure S6A). To confirm the expression of Hsp70 in elavGS;HSPA1L;HTTex1Q97 flies, we also analyzed protein extracts of hormone-treated animals by SDS-PAGE and immunoblotting. As expected, similar Hsp70 protein levels were detectable in head lysates of hormone-treated elavGS;HSPA1L;HTTex1Q97 and elavGS;HSPA1L control flies (Figure S6B).

Next, we assessed whether short-term co-expression of Hsp70 (for 6 days) in adult neurons influences the survival of elavGS;HSPA1L;HTTex1Q97 HD flies. In control experiments, the survival of short-term RU486-treated elavGS;HTTex1Q97 flies was analyzed. We determined median life spans of ~39 and ~33 days for RU486-treated elavGS;HSPA1L;HTTex1Q97 and elavGS;HTTex1Q97 flies, respectively, (Figures 6A–6C), indicating that short-term co-expression of Hsp70 in adult neurons improves the survival of elavGS;HSPA1L;HTTex1Q97 flies. As expected, a median life span of ~89 days was observed for non-treated elavGS;HTTex1Q97 flies, confirming our initial results (Figure 5C).

To examine whether short-term co-expression (6 days) of Hsp70 in adult neurons influences mHTTex1 aggregation, head lysates of 13-day-old RU486-treated elavGS;HSPA1L;HTTex1Q97 and elavGS;HTTex1Q97 flies were analyzed by FRAs and FRASE assays. We found that the abundance of large HTTex1Q97 aggregates and HSA were significantly decreased in brains of hormone-treated elavGS;HSPA1L;HTTex1Q97 flies in comparison to elavGS;HTTex1Q97 flies (Figures 6D–6F), substantiating our hypotheses that quantification of HSA predicts survival of HD transgenic flies.

Finally, we addressed the question whether the molecular chaperone Hsp70 associates directly with mHTTex1 aggregates in fly neurons. Immunohistochemical investigations of brains prepared from 9-day-old elavGS;HSPA1L;HTTex1Q97 flies treated for 6 days with RU486 revealed partial co-localization of Hsp70 and HTTex1Q97 aggregates (Figure 6G), supporting previous observations that Hsp70 directly targets aggregation-prone polyQ-containing HTTex1 fragments (Warrick et al., 1999).

Depletion of Hsc70 Increases Q35-YFP Seeding Activity in a *C. elegans* Model

Our studies in HD flies indicate that short-term overproduction of Hsp70 decreases HSA in neurons (Figure 6F), suggesting that a decrease of chaperone expression might have the opposite effect. To address this question, we performed RNAi knockdown experiments in transgenic worms that overproduce the aggregation-prone protein Q35-YFP in body wall muscle cells. Previous studies have demonstrated that Q35-YFP aggregation in these cells leads to motor impairment and that this phenotype increases in severity upon knockdown of *hsp-1* (Hsc70) gene expression by RNAi (Brehme et al., 2014). We treated Q35-YFP-expressing worms with *hsp-1* RNAi and assessed their motility at day 5. We observed a significant reduction of motility in RNAi-treated worms in comparison to untreated worms (Figure S6C), confirming previously published results (Brehme et al., 2014). Furthermore, this phenotypic change was associated with a significant increase in Q35-YFP seeding activity measured by FRASE assays (Figures S6D and S6E), supporting our hypothesis that HSA is a marker of dysfunction and toxicity in model systems.

DISCUSSION

There is increasing experimental evidence that self-propagating mHTT aggregates, or seeds, play an important role in HD model organisms (Babcock and Ganetzky, 2015; Pecho-Vrieseling et al., 2014). However, whether they are critical or even responsible for the appearance and progression of disease is still

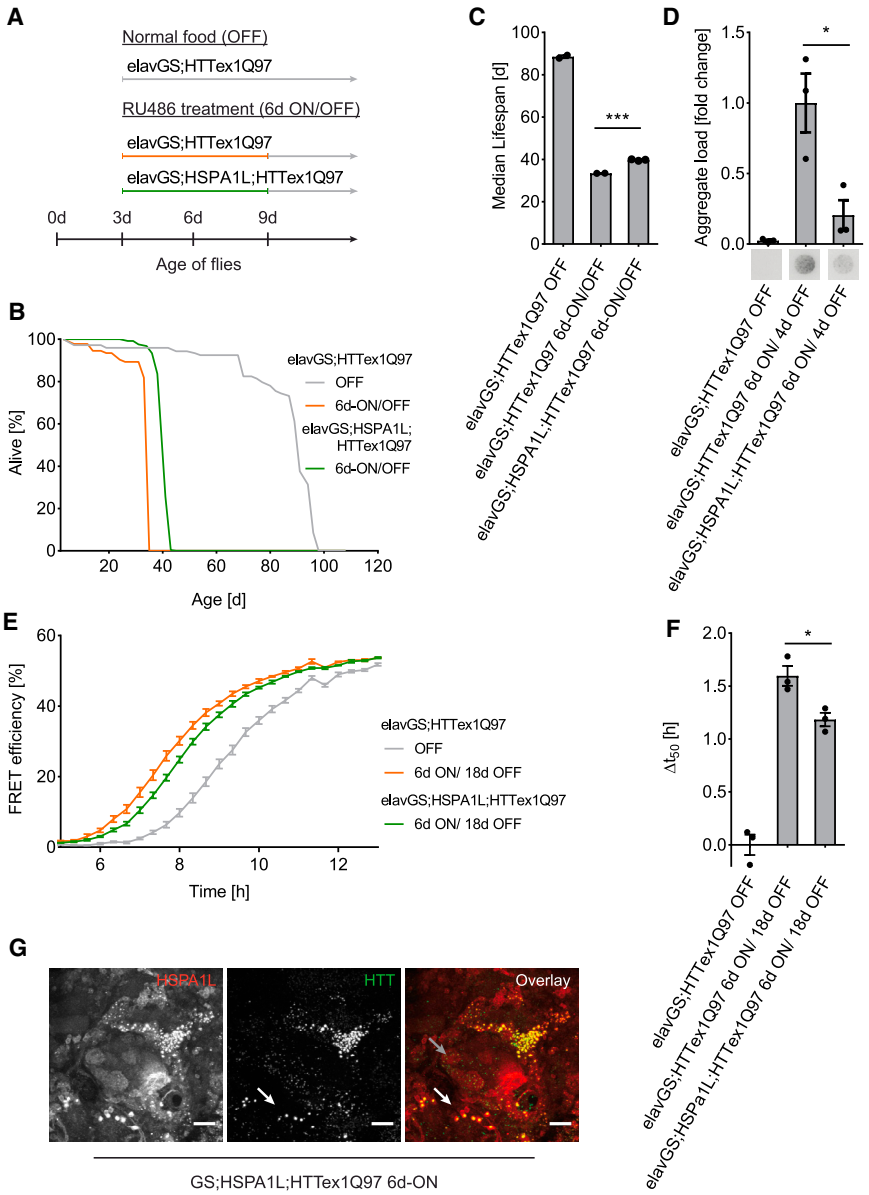

Figure 6. Co-production of Hsp70 Extends Survival of HD Flies

(A) Scheme depicting the workflow for the temporary treatment of HD transgenic flies with RU486.

(B) Life span analysis of short-term RU486-treated elavGS;HSPA1L;HTTex1Q97 flies (n = ~90 flies/group). Hormone-treated and untreated elavGS;HTTex1Q97 (n = ~40 flies/group) were also analyzed. Three biological replicates are shown.

(C) Median life span calculated from survival curves in (B). Error bars are mean ± SEM from three independent replicates. Unpaired t test.

(D) Quantification of large, SDS-stable HTTex1Q97 aggregates in fly heads by FRAs using the MW8 antibody. Representative images for each condition are shown. Data are mean ± SEM. Individual measurements are presented as dots (•). Unpaired t test.

(E) FRASE analysis of fly head lysates. Values are plotted as mean ± SEM of three biological replicates each performed in triplicate.

(F) Quantification of HSA from FRET-based aggregation profiles in (E). Data are mean ± SEM. Individual measurements are presented as dots (•). Unpaired t test.

(G) Representative confocal images of the right central brain region of elavGS;HSPA1L;HTTex1Q97 flies treated for 6 days with RU486 and immunostained for HTT (MAB5492, green) and Hsp70 (anti-HSP70/HSP72, red). White arrows indicate co-localization of Hsp70 with HTTex1 aggregates; the gray arrow indicates areas with no co-localization. Scale bars: 20 μm. See also Figure S6.

unclear. To address this question, we developed a sensitive FRET-based mHTT aggregate seeding (FRASE) assay that enables the quantification HSA in complex biosamples. With this assay in hand, we assessed the potential correlation between HSA in affected tissues and appearance of disease phenotypes in various HD models (Figures 3, 4, 5, and 6). For example, we detected HSA in crude brain extracts of mice weeks before manifestation of disease (Figures 3E–3G). Furthermore, we observed an increase of mutant HSA in mouse brain extracts concomitantly with the appearance of symptoms, suggesting that it quantitatively tracks disease progression. Finally, mechanistic studies with a newly established inducible *Drosophila* model of HD indicate a correlation between HSA in adult neurons and reduced survival of HD flies, supporting our hypothesis that mHTT seeding is a disease-relevant process. Altogether, these studies indicate that HSA is a valuable early disease marker that can predict severe downstream phenotypic changes in various HD models.

The fluorescent dye ThT is used in a large number of cell-free assays as a reporter molecule to monitor the seeding activity of amyloidogenic protein aggregates (Gupta et al., 2012). ThT exhibits enhanced fluorescence when it is bound to β-sheet-rich amyloid structures (LeVine, 1993). However, its binding to such structures is significantly decreased when competing proteins are present in complex amyloid polymerization reactions (Biancalana and Koide, 2010). Therefore, previously established ThT-based seeding assays are relatively insensitive when biosamples such as brain homogenates are analyzed (Gupta et al., 2012). To overcome these limitations, we have established the FRASE assay, which does not require ThT reporter molecules for the quantification of HSA in biosamples. Two fluorescently tagged aggregation-prone HTTex1 fusion proteins are used as reporter molecules to monitor HSA (Figure 3A). This assay is highly robust and affected by contaminating proteins in complex biosamples only to a small extent. Therefore, the FRASE assay can be employed without the need for

upstream purification of mHTT seeds, which would complicate the protocol and decrease the accuracy of quantification.

We observed high HSA in soluble fractions of HD mouse brain extracts (Figures 4B and 4C), suggesting that seeding activity in transgenic animals predominately originates from small, rather than large, mHTTex1 aggregates. However, inclusions with insoluble fibrillar HTTex1 aggregates (Bauerlein et al., 2017) may also possess seeding activity. Further studies will be necessary to purify fibrillar HTTex1 structures of different sizes from mouse and fly brains and to compare their specific seeding activity (i.e., seeding activity per unit of protein). Our results agree with previous investigations indicating that small, fibrillar polyQ-containing HTT assemblies are detectable in the cytoplasm of cells, in addition to large inclusions with fibrillar mHTT aggregates (Sahl et al., 2012). They are also consistent with studies demonstrating that proteotoxicity in mammalian cells is associated with small, diffusible HTT oligomers, rather than large inclusions (Arrasate et al., 2004; Leitman et al., 2013). However, our study advances beyond the state of the art. For the first time, we provide experimental evidence that the abundance of small seeding-competent polyQ structures correlates with dysfunction and toxicity in HD transgenic flies and worms (Figures 5, 6, and S6).

Altogether, our investigations suggest that HSA in HD mouse and fly brain extracts is a biological marker of disease long before its onset. Previous studies argue that large inclusions with insoluble mHTT aggregates in brains of HD mice and patients are not predictive for the development of symptoms (Kuemmerle et al., 1999). However, neuronal inclusions are commonly detected with immunohistological methods, which fail to identify small, seeding-competent mHTT assemblies. The application of the FRASE assay overcomes this important limitation associated with standard histology and is likely to yield new mechanistic insights into the progressive development of HD. We propose that in future drug trials with HD mice, HSA could be used as an outcome marker to monitor the efficacy of therapeutic molecules *in vivo*, before and independent of changes in phenotype. Because we detected robust HSA in the striatum of 2-month-old *Hdh*Q150 knockin mice (Figure 3G), drug treatment could start before that time and animals could be assessed for HSA at any later age. Furthermore, we propose that the FRASE method can be applied as a drug screening assay to identify therapeutic molecules that directly target mHTT seeding *in vitro*. Because the assay can monitor HSA in protein extracts prepared from postmortem patient brains and transgenic animals (Figures 3D–3G), it seems feasible to investigate aggregate-targeting therapeutic candidate molecules in assays that contain disease-relevant seeds.

Through the application of FRASE assays, we have demonstrated that HSA is a robust, early disease biomarker in HD transgenic mice and flies. We propose that it also might be of high value for monitoring disease onset and progression in HD patients if HSA could be quantified in biosamples whose collection is technically and ethically possible, like cerebrospinal fluid, blood, or muscle tissue. Through the quantification of HSA in patient samples, the optimal time point for the initiation of clinical trials could be determined and the efficacy of therapeutic interventions could be monitored. In this way, our findings may help to develop novel disease-modifying therapeutic strategies for HD and other polyQ diseases.

STAR★METHODS

Detailed methods are provided in the online version of this paper and include the following:

- KEY RESOURCES TABLE
- CONTACT FOR REAGENT AND RESOURCE SHARING
- EXPERIMENTAL MODEL AND SUBJECT DETAILS
  - HD mouse models
  - Human brain tissue
  - Generation and maintenance of *Drosophila* strains
  - *C. elegans* strains and maintenance
- METHOD DETAILS
  - Cloning of expression vectors
  - Recombinant protein expression
  - Preparation of *in vitro* seeds
  - Atomic force microscopy
  - Filter retardation assays
  - Dot blot assays
  - Native gels
  - SDS-PAGE and Western blotting
  - Genotyping of *Drosophila* strains
  - Quantitative polymerase chain reaction (qPCR)
  - Viability analysis of adult *Drosophila melanogaster*
  - Analysis of motor performance (climbing assay)
  - Preparation of *Drosophila* head lysates for FRAs
  - Dissection and immunostaining of *Drosophila* adult brain
  - RNA interference
  - Fluorescence microscopy
  - Motility assay
  - Tissue homogenization
  - Electron microscopy
  - Immunodepletion of HTTex1 aggregates from mouse brain extracts
  - FRASE assay
  - Quantification of mHTT seeding activity (HSA)
- QUANTIFICATION AND STATISTICAL ANALYSIS

SUPPLEMENTAL INFORMATION

Supplemental Information includes six figures and can be found with this article online at https://doi.org/10.1016/j.molcel.2018.07.032.

ACKNOWLEDGMENTS

pBAD33-CyPet-His and pBAD33-YPet-His were gifts from P.S. Daugherty, University of California, Santa Barbara, USA. The expression vector for Tau pRK172 Tau40 was obtained from M. Goedert, MRC Laboratory of Molecular Biology, Cambridge, UK. Human brain tissue was provided by the Newcastle Brain Tissue Resource (NBTR), which is funded in part by a grant from the UK Medical Research Council (G0400074) and by Brains for Dementia Research, a joint venture between Alzheimer's Society and Alzheimer's Research UK. This work was supported by the HDSA (to A.B.), the Swedish Research Council (to Å.P.), and the CHDI Foundation (to E.E.W., G.P.B., and A.J.M.). In addition, this study received funding from the EC funding initiative ERA-NET NEURON,

consortium "ABETA ID," funded by the German Federal Ministry for Education and Research (BMBF) (01W1301); the Berlin Institute of Health Collaborative Research (1.1.2.a.3, "Elucidating the Proteostasis Network to Control Alzheimer's Disease"), funded by the German Federal Ministry for Education and Research (BMBF); the Helmholtz Validation Fund (HVF-0013, "Enabling Technologies for Drug Discovery against Protein Misfolding Diseases"), funded by the Helmholtz Association, Germany (to E.E.W.); the Stiftung Charité (to E.E.W.); and the Max Delbrück Center for Molecular Medicine in the Helmholtz Association for application-oriented research (to A. Boeddrich and E.E.W.). We thank M. van Waarde-Verhagen, Z. Zheng, and M. Harding for excellent technical assistance. We thank the Advanced Light Microscopy Technology Platform of Max-Delbrück-Center for Molecular Medicine, Berlin, for the general and technical support. Finally, we thank T. Vogt and I. Munoz-Sanjuan (both of CHDI) for their interest and support of this project. Icons used in Figure 3A were taken from Freepik.

AUTHOR CONTRIBUTIONS

A. Buntru, A.A., F.S., and E.E.W. conceived the study and designed the experiments; A. Buntru, A.A., and F.S. analyzed the data. A.A., R.H., I.J., and K.K. performed experiments with *in vitro* seeds. A.A. and R.H. performed mouse and human tissue experiments. F.S., A.A., L.B., and J.E. performed all studies with the HD transgenic flies. L.D. and A. Boeddrich performed aggregation experiments with non-polyQ proteins. R.H. performed immunodepletion experiments and FRAs. A.S. and A.G. performed toxicity assays with primary neurons. S.K. and B.P. labeled and analyzed EM samples. J.K. performed all experiments with nematodes. L.B. analyzed protease cleavage reactions with SDS-PAGE. B.M. performed experiments with AAV5 HTT853-injected mice. H.N. performed cell culture studies. H.H.K. provided cell lines. B.B. and Å.P. performed the injections of AAV vectors in FVBN/mice and provided samples. A.J.M. coordinated breeding of R6/2Q51 mice and provided samples. S.A.F. and G.P.B. coordinated breeding of R6/2Q212 and *Hdh*Q150 mice and provided samples. L.B. and G.G. analyzed AFM samples. E.E.W., A. Buntru, A.A., and S.S. conceived and wrote the manuscript.

DECLARATION OF INTERESTS

The authors declare no competing interests.

Received: December 21, 2016
Revised: November 10, 2017
Accepted: July 24, 2018
Published: September 6, 2018

REFERENCES

Arrasate, M., Mitra, S., Schweitzer, E.S., Segal, M.R., and Finkbeiner, S. (2004). Inclusion body formation reduces levels of mutant huntingtin and the risk of neuronal death. Nature *431*, 805–810.

Atarashi, R., Moore, R.A., Sim, V.L., Hughson, A.G., Dorward, D.W., Onwubiko, H.A., Priola, S.A., and Caughey, B. (2007). Ultrasensitive detection of scrapie prion protein using seeded conversion of recombinant prion protein. Nat. Methods *4*, 645–650.

Atarashi, R., Satoh, K., Sano, K., Fuse, T., Yamaguchi, N., Ishibashi, D., Matsubara, T., Nakagaki, T., Yamanaka, H., Shirabe, S., et al. (2011). Ultrasensitive human prion detection in cerebrospinal fluid by real-time quaking-induced conversion. Nat. Med. *17*, 175–178.

Babcock, D.T., and Ganetzky, B. (2015). Transcellular spreading of huntingtin aggregates in the *Drosophila* brain. Proc. Natl. Acad. Sci. USA *112*, E5427–E5433.

Baldo, B., Soylu, R., and Petersén, A. (2013). Maintenance of basal levels of autophagy in Huntington's disease mouse models displaying metabolic dysfunction. PLoS ONE *8*, e83050.

Bauerlein, F.J.B., Saha, I., Mishra, A., Kalemanov, M., Martinez-Sanchez, A., Klein, R., Dudanova, I., Hipp, M.S., Hartl, F.U., Baumeister, W., et al. (2017). In Situ Architecture and Cellular Interactions of PolyQ Inclusions. Cell *171*, 179–187.

Biancalana, M., and Koide, S. (2010). Molecular mechanism of Thioflavin-T binding to amyloid fibrils. Biochim. Biophys. Acta *1804*, 1405–1412.

Bischof, J., Maeda, R.K., Hediger, M., Karch, F., and Basler, K. (2007). An optimized transgenesis system for Drosophila using germ-line-specific phiC31 integrases. Proc. Natl. Acad. Sci. USA *104*, 3312–3317.

Brehme, M., Voisine, C., Rolland, T., Wachi, S., Soper, J.H., Zhu, Y., Orton, K., Villella, A., Garza, D., Vidal, M., et al. (2014). A chaperome subnetwork safeguards proteostasis in aging and neurodegenerative disease. Cell Rep. *9*, 1135–1150.

Brundin, P., Melki, R., and Kopito, R. (2010). Prion-like transmission of protein aggregates in neurodegenerative diseases. Nat. Rev. Mol. Cell Biol. *11*, 301–307.

Carter, R.J., Lione, L.A., Humby, T., Mangiarini, L., Mahal, A., Bates, G.P., Dunnett, S.B., and Morton, A.J. (1999). Characterization of progressive motor deficits in mice transgenic for the human Huntington's disease mutation. J. Neurosci. *19*, 3248–3257.

Castilla, J., Saá, P., and Soto, C. (2005). Detection of prions in blood. Nat. Med. *11*, 982–985.

Chan, H.Y., Warrick, J.M., Gray-Board, G.L., Paulson, H.L., and Bonini, N.M. (2000). Mechanisms of chaperone suppression of polyglutamine disease: selectivity, synergy and modulation of protein solubility in *Drosophila*. Hum. Mol. Genet. *9*, 2811–2820.

Chiti, F., and Dobson, C.M. (2017). Protein misfolding, amyloid formation, and human disease: a summary of progress over the last decade. Annu. Rev. Biochem. *86*, 27–68.

Ciamei, A., Detloff, P.J., and Morton, A.J. (2015). Progression of behavioural despair in R6/2 and Hdh knock-in mouse models recapitulates depression in Huntington's disease. Behav. Brain Res. *291*, 140–146.

Cohen, S.I., Vendruscolo, M., Dobson, C.M., and Knowles, T.P. (2012). From macroscopic measurements to microscopic mechanisms of protein aggregation. J. Mol. Biol. *421*, 160–171.

Davies, S.W., Turmaine, M., Cozens, B.A., DiFiglia, M., Sharp, A.H., Ross, C.A., Scherzinger, E., Wanker, E.E., Mangiarini, L., and Bates, G.P. (1997). Formation of neuronal intranuclear inclusions underlies the neurological dysfunction in mice transgenic for the HD mutation. Cell *90*, 537–548.

DiFiglia, M., Sapp, E., Chase, K.O., Davies, S.W., Bates, G.P., Vonsattel, J.P., and Aronin, N. (1997). Aggregation of huntingtin in neuronal intranuclear inclusions and dystrophic neurites in brain. Science *277*, 1990–1993.

Du, D., Murray, A.N., Cohen, E., Kim, H.E., Simkovsky, R., Dillin, A., and Kelly, J.W. (2011). A kinetic aggregation assay allowing selective and sensitive amyloid-β quantification in cells and tissues. Biochemistry *50*, 1607–1617.

Gao, M., Estel, K., Seeliger, J., Friedrich, R.P., Dogan, S., Wanker, E.E., Winter, R., and Ebbinghaus, S. (2015). Modulation of human IAPP fibrillation: cosolutes, crowders and chaperones. Phys. Chem. Chem. Phys. *17*, 8338–8348.

Guo, J.L., and Lee, V.M. (2014). Cell-to-cell transmission of pathogenic proteins in neurodegenerative diseases. Nat. Med. *20*, 130–138.

Gupta, S., Jie, S., and Colby, D.W. (2012). Protein misfolding detected early in pathogenesis of transgenic mouse model of Huntington disease using amyloid seeding assay. J. Biol. Chem. *287*, 9982–9989.

Herva, M.E., Zibaee, S., Fraser, G., Barker, R.A., Goedert, M., and Spillantini, M.G. (2014). Anti-amyloid compounds inhibit α-synuclein aggregation induced by protein misfolding cyclic amplification (PMCA). J. Biol. Chem. *289*, 11897–11905.

Hockly, E., Woodman, B., Mahal, A., Lewis, C.M., and Bates, G. (2003). Standardization and statistical approaches to therapeutic trials in the R6/2 mouse. Brain Res. Bull. *61*, 469–479.

Holmes, B.B., Furman, J.L., Mahan, T.E., Yamasaki, T.R., Mirbaha, H., Eades, W.C., Belaygorod, L., Cairns, N.J., Holtzman, D.M., and Diamond, M.I. (2014).

Proteopathic tau seeding predicts tauopathy *in vivo*. Proc. Natl. Acad. Sci. USA *111*, E4376–E4385.

Hult, S., Soylu, R., Björklund, T., Belgardt, B.F., Mauer, J., Brüning, J.C., Kirik, D., and Petersén, Å. (2011). Mutant huntingtin causes metabolic imbalance by disruption of hypothalamic neurocircuits. Cell Metab. *13*, 428–439.

Jarrett, J.T., and Lansbury, P.T., Jr. (1993). Seeding "one-dimensional crystallization" of amyloid: a pathogenic mechanism in Alzheimer's disease and scrapie? Cell *73*, 1055–1058.

Jeon, I., Cicchetti, F., Cisbani, G., Lee, S., Li, E., Bae, J., Lee, N., Li, L., Im, W., Kim, M., et al. (2016). Human-to-mouse prion-like propagation of mutant huntingtin protein. Acta Neuropathol. *132*, 577–592.

Jiang, X., and Sorkin, A. (2002). Coordinated traffic of Grb2 and Ras during epidermal growth factor receptor endocytosis visualized in living cells. Mol. Biol. Cell *13*, 1522–1535.

Jucker, M., and Walker, L.C. (2013). Self-propagation of pathogenic protein aggregates in neurodegenerative diseases. Nature *501*, 45–51.

Kayed, R., Head, E., Thompson, J.L., McIntire, T.M., Milton, S.C., Cotman, C.W., and Glabe, C.G. (2003). Common structure of soluble amyloid oligomers implies common mechanism of pathogenesis. Science *300*, 486–489.

Ko, J., Ou, S., and Patterson, P.H. (2001). New anti-huntingtin monoclonal antibodies: implications for huntingtin conformation and its binding proteins. Brain Res. Bull. *56*, 319–329.

Kuemmerle, S., Gutekunst, C.A., Klein, A.M., Li, X.J., Li, S.H., Beal, M.F., Hersch, S.M., and Ferrante, R.J. (1999). Huntington aggregates may not predict neuronal death in Huntington's disease. Ann. Neurol. *46*, 842–849.

Larson, E., Fyfe, I., Morton, A.J., and Monckton, D.G. (2015). Age-, tissue- and length-dependent bidirectional somatic CAG·CTG repeat instability in an allelic series of R6/2 Huntington disease mice. Neurobiol. Dis. *76*, 98–111.

Latouche, M., Lasbleiz, C., Martin, E., Monnier, V., Debeir, T., Mouatt-Prigent, A., Muriel, M.P., Morel, L., Ruberg, M., Brice, A., et al. (2007). A conditional pan-neuronal *Drosophila* model of spinocerebellar ataxia 7 with a reversible adult phenotype suitable for identifying modifier genes. J. Neurosci. *27*, 2483–2492.

Laue, M. (2010). Electron microscopy of viruses. Methods Cell Biol. *96*, 1–20.

Leitman, J., Ulrich Hartl, F., and Lederkremer, G.Z. (2013). Soluble forms of polyQ-expanded huntingtin rather than large aggregates cause endoplasmic reticulum stress. Nat. Commun. *4*, 2753.

LeVine, H., 3rd (1993). Thioflavine T interaction with synthetic Alzheimer's disease beta-amyloid peptides: detection of amyloid aggregation in solution. Protein Sci. *2*, 404–410.

Li, H., Li, S.H., Cheng, A.L., Mangiarini, L., Bates, G.P., and Li, X.J. (1999). Ultrastructural localization and progressive formation of neuropil aggregates in Huntington's disease transgenic mice. Hum. Mol. Genet. *8*, 1227–1236.

Lin, C.H., Tallaksen-Greene, S., Chien, W.M., Cearley, J.A., Jackson, W.S., Crouse, A.B., Ren, S., Li, X.J., Albin, R.L., and Detloff, P.J. (2001). Neurological abnormalities in a knock-in mouse model of Huntington's disease. Hum. Mol. Genet. *10*, 137–144.

Lin, D.M., and Goodman, C.S. (1994). Ectopic and increased expression of Fasciclin II alters motoneuron growth cone guidance. Neuron *13*, 507–523.

Liu, K.S.Y., Siebert, M., Mertel, S., Knoche, E., Wegener, S., Wichmann, C., Matkovic, T., Muhammad, K., Depner, H., Mettke, C., et al. (2011). RIM-binding protein, a central part of the active zone, is essential for neurotransmitter release. Science *334*, 1565–1569.

Mangiarini, L., Sathasivam, K., Seller, M., Cozens, B., Harper, A., Hetherington, C., Lawton, M., Trottier, Y., Lehrach, H., Davies, S.W., and Bates, G.P. (1996). Exon 1 of the HD gene with an expanded CAG repeat is sufficient to cause a progressive neurological phenotype in transgenic mice. Cell *87*, 493–506.

Nguyen, A.W., and Daugherty, P.S. (2005). Evolutionary optimization of fluorescent proteins for intracellular FRET. Nat. Biotechnol. *23*, 355–360.

Nucifora, L.G., Burke, K.A., Feng, X., Arbez, N., Zhu, S., Miller, J., Yang, G., Ratovitski, T., Delannoy, M., Muchowski, P.J., et al. (2012). Identification of novel potentially toxic oligomers formed *in vitro* from mammalian-derived expanded huntingtin exon-1 protein. J. Biol. Chem. *287*, 16017–16028.

Osterwalder, T., Yoon, K.S., White, B.H., and Keshishian, H. (2001). A conditional tissue-specific transgene expression system using inducible GAL4. Proc. Natl. Acad. Sci. USA *98*, 12596–12601.

Pecho-Vrieseling, E., Rieker, C., Fuchs, S., Bleckmann, D., Esposito, M.S., Botta, P., Goldstein, C., Bernhard, M., Galimberti, I., Müller, M., et al. (2014). Transneuronal propagation of mutant huntingtin contributes to non-cell autonomous pathology in neurons. Nat. Neurosci. *17*, 1064–1072.

Pearce, M.M., Spartz, E.J., Hong, W., Luo, L., and Kopito, R.R. (2015). Prion-like transmission of neuronal huntingtin aggregates to phagocytic glia in the Drosophila brain. Nat. Commun. *6*, 6768.

Pieri, L., Madiona, K., Bousset, L., and Melki, R. (2012). Fibrillar α-synuclein and huntingtin exon 1 assemblies are toxic to the cells. Biophys. J. *102*, 2894–2905.

Rogers, I., Kerr, F., Martinez, P., Hardy, J., Lovestone, S., and Partridge, L. (2012). Ageing increases vulnerability to abeta42 toxicity in Drosophila. PLoS ONE *7*, e40569.

Saborio, G.P., Permanne, B., and Soto, C. (2001). Sensitive detection of pathological prion protein by cyclic amplification of protein misfolding. Nature *411*, 810–813.

Sahl, S.J., Weiss, L.E., Duim, W.C., Frydman, J., and Moerner, W.E. (2012). Cellular inclusion bodies of mutant huntingtin exon 1 obscure small fibrillar aggregate species. Sci. Rep. *2*, 895.

Sathasivam, K., Neueder, A., Gipson, T.A., Landles, C., Benjamin, A.C., Bondulich, M.K., Smith, D.L., Faull, R.L., Roos, R.A., Howland, D., et al. (2013). Aberrant splicing of HTT generates the pathogenic exon 1 protein in Huntington disease. Proc. Natl. Acad. Sci. USA *110*, 2366–2370.

Scherzinger, E., Lurz, R., Turmaine, M., Mangiarini, L., Hollenbach, B., Hasenbank, R., Bates, G.P., Davies, S.W., Lehrach, H., and Wanker, E.E. (1997). Huntingtin-encoded polyglutamine expansions form amyloid-like protein aggregates *in vitro* and *in vivo*. Cell *90*, 549–558.

Scherzinger, E., Sittler, A., Schweiger, K., Heiser, V., Lurz, R., Hasenbank, R., Bates, G.P., Lehrach, H., and Wanker, E.E. (1999). Self-assembly of polyglutamine-containing huntingtin fragments into amyloid-like fibrils: implications for Huntington's disease pathology. Proc. Natl. Acad. Sci. USA *96*, 4604–4609.

Schindelin, J., Arganda-Carreras, I., Frise, E., Kaynig, V., Longair, M., Pietzsch, T., Preibisch, S., Rueden, C., Saalfeld, S., Schmid, B., et al. (2012). Fiji: an open-source platform for biological-image analysis. Nat. Methods *9*, 676–682.

Stewart, B.A., Atwood, H.L., Renger, J.J., Wang, J., and Wu, C.F. (1994). Improved stability of *Drosophila* larval neuromuscular preparations in haemolymph-like physiological solutions. J. Comp. Physiol. A Neuroethol. Sens. Neural Behav. Physiol. *175*, 179–191.

Tan, Z., Dai, W., van Erp, T.G., Overman, J., Demuro, A., Digman, M.A., Hatami, A., Albay, R., Sontag, E.M., Potkin, K.T., et al. (2015). Huntington's disease cerebrospinal fluid seeds aggregation of mutant huntingtin. Mol. Psychiatry *20*, 1286–1293.

Theillet, F.X., Binolfi, A., Bekei, B., Martorana, A., Rose, H.M., Stuiver, M., Verzini, S., Lorenz, D., van Rossum, M., Goldfarb, D., and Selenko, P. (2016). Structural disorder of monomeric α-synuclein persists in mammalian cells. Nature *530*, 45–50.

Wagner, A.S., Politi, A.Z., Ast, A., Bravo-Rodriguez, K., Baum, K., Buntru, A., Strempel, N.U., Brusendorf, L., Hänig, C., Boeddrich, A., et al. (2018). Self-assembly of mutant huntingtin exon-1 fragments into large complex fibrillar structures involves nucleated branching. J. Mol. Biol. *430*, 1725–1744.

Wanker, E.E., Scherzinger, E., Heiser, V., Sittler, A., Eickhoff, H., and Lehrach, H. (1999). Membrane filter assay for detection of amyloid-like polyglutamine-containing protein aggregates. Methods Enzymol. *309*, 375–386.

Warrick, J.M., Chan, H.Y., Gray-Board, G.L., Chai, Y., Paulson, H.L., and Bonini, N.M. (1999). Suppression of polyglutamine-mediated

neurodegeneration in *Drosophila* by the molecular chaperone HSP70. Nat. Genet. *23*, 425–428.

Woodman, B., Butler, R., Landles, C., Lupton, M.K., Tse, J., Hockly, E., Moffitt, H., Sathasivam, K., and Bates, G.P. (2007). The Hdh(Q150/Q150) knock-in mouse model of HD and the R6/2 exon 1 model develop comparable and widespread molecular phenotypes. Brain Res. Bull. *72*, 83–97.

Zhang, J.H., Chung, T.D., and Oldenburg, K.R. (1999). A simple statistical parameter for use in evaluation and validation of high throughput screening assays. J. Biomol. Screen. *4*, 67–73.

Zuccato, C., Valenza, M., and Cattaneo, E. (2010). Molecular mechanisms and potential therapeutical targets in Huntington's disease. Physiol. Rev. *90*, 905–981.

STAR★METHODS

KEY RESOURCES TABLE

REAGENT or RESOURCE	SOURCE	IDENTIFIER
Antibodies		
Rabbit polyclonal anti-GFP	Abcam	Cat#: ab290; RRID:AB_303395
Rabbit polyclonal anti-HTT (HD1)	Own production	Scherzinger et al., 1999
Mouse monoclonal anti-HTT (clone MW8)	DSHB	Cat#: MW8; RRID:AB_528297
Rabbit polyclonal anti-Agg53	This study	N/A
Goat polyclonal anti-HTT (N18)	Santa Cruz	Cat#: sc-8767; RRID:AB_2123254
Mouse monoclonal anti-HTT (clone 2B4)	Merck Millipore	Cat#: MAB5492; RRID:AB_347723
Rabbit polyclonal anti-HSP70/HSP72	Enzo Life Science	Cat#: ADI-SPA-812-D; RRID:AB_11180512
Bacterial and Virus Strains		
BL21-CodonPlus(DE3)-RP	Integrated Science	Cat#: 230255
Biological Samples		
Post mortem brain tissues from human HD and AD patients and unaffected control individuals	Newcastle Brain Tissue Resource	N/A
Chemicals, Peptides, and Recombinant Proteins		
GST-HTTex1Q23	This study	N/A
GST-HTTex1Q48	(Wagner et al., 2018)	N/A
GST-HTTex1Q23-CyPet	This paper	N/A
GST-HTTex1Q23-YPet	This paper	N/A
GST-HTTex1Q48-CyPet	(Wagner et al., 2018)	N/A
GST-HTTex1Q48-YPet	(Wagner et al., 2018)	N/A
αSyn	(Theillet et al., 2016)	N/A
Tau40	InVivo BioTech Services	N/A
Mifepristone RU486	Sigma	Cat#: M8046-1G
M-MLV Reverse Transcriptase	Thermo Scientific	Cat#: 28025013
Critical Commercial Assays		
Pierce BCA Protein Assay Kit	Thermo Scientific	Cat#: 23225
DNeasy® Blood & Tissue Kit	QIAGEN	Cat#: 69504
TRIzol Reagent	Invitrogen	Cat#: 15596026
SYBR Green PCR Master Mix	Thermo Scientific	Cat#: 4309155
Experimental Models: Organisms/Strains		
Mouse: R6/2Q210	(Mangiarini et al., 1996)	N/A
Mouse: CBA x C57BL/6	Harlan Olac, Bicester, UK	B6CBAF1/OlaHsd
Mouse: *Hdh*Q150	(Lin et al., 2001)	N/A
Mouse: R6/2Q51	(Larson et al., 2015)	N/A
Mouse: FVB/N with AAV-HTT853-Q79/Q18	(Baldo et al., 2013)	N/A
Fly: $Elav^{c115}$-GAL4	(Lin and Goodman, 1994)	N/A
Fly: GSelav-GAL4	Bloomington Drosophila Stock Center	Bloomington Stock 43642
Fly: HTTex1Q17	This study	N/A
Fly: HTTex1Q97	This study	N/A
Fly: HSPA1L	(Warrick et al., 1999)	N/A

(*Continued on next page*)

Continued

REAGENT or RESOURCE	SOURCE	IDENTIFIER
Oligonucleotides		
HTTex1Q48 no Stop forward primer: 5′-gacgacgaattcatggcgaccctg-3′	This study	N/A
HTTex1Q48 no Stop reverse primer: 5′-gacgacctcgag tggtcggtgcagcgg-3′	This study	N/A
CyPet forward primer: 5′-acgacctcgagggtggcggtgg cggtatgtctaaag gtgaagaattattcgg-3′	This study	N/A
CyPet reverse primer: 5′- gacgacgcggccgcttatttgtacaat tcatccatacc atg-3′	This study	N/A
YPet forward primer: 5′-gacgacctcgagggtggcggtgg cggtatgtctaaa ggtgaagaattattcactgg-3′	This study	N/A
YPet reverse primer: 5′- gacgacgcggccgcttatttgtaca attcattcataccc tcg-3′	This study	N/A
HTTex1Q23 no Stop forward primer: 5′-gacgacgaatt catggcgaccctg-3′	This study	N/A
HTTex1Q23 no Stop reverse primer: 5′-gacgacgcggccg cctcgagtggtcggtg cagcgg-3′	This study	N/A
HTTex1Q23 forward primer: 5′gacgacgaattcatggcg accctg −3′	This study	N/A
HTTex1Q23 reverse primer: 5′-gacgacgcggccgcctcga gttatggtcggtgcagcgg-3′	This study	N/A
Drosophila genotyping forward primer: 5′-aaccccgtaaa tcaactgc- 3′	This study	N/A
Drosophila genotyping reverse primer: 5′-atctctgtaggt agtttgtc-3′	This study	N/A
HTTqPCR forward primer: 5′-gacctggaaaagctgatga-3′	This study	N/A
HTTqPCR reverse primer: 5′-tcatggtcggtgcagcggct-3′	This study	N/A
rp49qPCR forward primer: 5′-tacaggcccaagatcgtgaa-3′	This study	N/A
rp49qPCR reverse primer: 5′-acgttgtgcaccaggaactt-3′	This study	N/A
Recombinant DNA		
pBAD33-CyPet-His	(Nguyen and Daugherty, 2005)	Addgene plasmid #14030
pBAD33-YPet-His	(Nguyen and Daugherty, 2005)	Addgene plasmid #14031
Software and Algorithms		
AIDA Image Analyzer v.3.21A	AIDA	N/A
GraphPad Prism	GraphPad software	N/A
JPK SPM software	JPK Instruments	N/A

CONTACT FOR REAGENT AND RESOURCE SHARING

Further information and requests for reagents may be directed to and will be fulfilled by the corresponding author, Erich E. Wanker (ewanker@mdc-berlin.de).

EXPERIMENTAL MODEL AND SUBJECT DETAILS

HD mouse models

Hemizygous R6/2Q212 mice (Mangiarini et al., 1996) were bred by backcrossing R6/2Q212 males to (CBA/Ca x C57BL/6J) F1 females (B6CBAF1/OlaHsd, Harlan Olac, Bicester, UK). *Hdh*Q150 heterozygous knock-in mice (Lin et al., 2001; Woodman et al., 2007) on a (CBA/Ca x C57BL/6J) F1 background were generated by intercrossing *Hdh*Q150 heterozygous CBA/Ca and C57BL/6J congenic lines (inbred lines from Harlan Olac, Bicester, UK). All animals were subject to a 12 h light/dark cycle with unlimited access to drinking water and breeding chow (Special Diet Services, Witham, UK). Housing conditions and environmental enrichment were described previously (Hockly et al., 2003). R6/2 mice were always housed with wild-type mice. The CAG repeat size of the

R6/2Q212 mice used in this study was 212 ± 5.27 (s.d.) and that of the *Hdh*Q150 heterozygotes was 160 ± 2.86 (s.d.). Hemizygous R6/2Q51 mice were derived from R6/2 parent lines by selective breeding (Larson et al., 2015) and bred by backcrossing R6/2Q51 males to (CBA x C57BL/6) F1 females (Charles Rivers, UK). R6/2Q51 mice were maintained and bred as described previously (Larson et al., 2015). Female mice from the FVB/N strain (Charles River Laboratories, Germany) were injected at eight to ten weeks of age with recombinant adeno-associated viral (AAV) vectors of serotype 5 encoding the first 853 amino acids of either the WT form of HTT with 18Q (HTT853- Q18) or the mutant form of the protein with 79Q (HTT853-Q97) (Baldo et al., 2013). All mice were housed in groups at a 12 h light/dark cycle. At 8 weeks post-injection, FVB/N mice were sacrificed. Overall, mice were sacrificed at different ages from 1 day up to 2 years. Tissues were strictly stored at −80°C until use.

All animal work with R6/2Q212 and *Hdh*Q150mice was approved by the King's College London Ethical Review panel and performed under a Home Office project license in accordance with the United Kingdom 1986 Animals (Scientific procedures) Act. All animal work with R6/2Q51 mice was approved by the University of Cambridge Ethical Review panel and performed under a Home Office project license in accordance with the United Kingdom 1986 Animals (Scientific procedures) Act. All experimental procedures with FVB/N mice were approved by the Regional Ethical Committee in Lund, Sweden.

Human brain tissue

Post mortem brain tissues from human HD and AD patients and unaffected control individuals (both male and female) were obtained from the Newcastle Brain Tissue Resource (NBTR, Newcastle University, UK). Experiments were performed in accordance with the approval of the joint Ethics Committee of Newcastle and North Tyneside Health Authority and following NBTR brain banking procedures. Tissues were collected at 34.5 ± 21.0 h post-mortem from HD patients and controls with an average age of 57.8 ± 10.7 years.

Generation and maintenance of *Drosophila* strains

ElavGS-GAL4, Elav-GAL4 and HSPA1L lines were obtained from the Bloomington *Drosophila* Stock Center. Transgenic flies were generated through cloning of cDNAs encoding HTTex1Q17 and HTTex1Q97 into pUAST-attB-rfA (provided by Prof. S. Sigrist, Freie Universität, Berlin) and subsequent site-directed insertion on the third chromosome (68E) using the PhiC31 integrase [Rainbow Transgenic Flies Inc. (Camarillo, CA, USA)]. All *Drosophila* strains were cultured on standard medium at 25°C and 65% humidity with a 12 h light-dark cycle. Expression of transgenes was induced by culturing flies on standard medium containing 400 μM RU486.

C. elegans strains and maintenance

C. elegans Q35 AM140 (rmIs132 (*unc*-54p::Q35::YFP)) were grown on NGM plates seeded with the *E. coli* OP50 strain at 20°C. Nematodes were transferred to fresh wells or plates every day in the course of the experiment to separate them from their progeny.

METHOD DETAILS

Cloning of expression vectors

For the construction of plasmids encoding CyPet- and YPet-tagged HTTEx1Q48 fusion proteins, the coding sequence of HTTEx1Q48 was PCR-amplified from pGEX-6P1-HTTEx1Q48 using the primers 5′-gacgacgaattcatggcgaccctg-3′ and 5′- gac gacctcgagtggtcggtgcagcgg-3′. The resulting PCR product was digested with the restriction enzymes EcoRI and NotI. Additionally, CyPet cDNA was PCR amplified from pBAD33-CyPet-His (Addgene plasmid #14030) (Nguyen and Daugherty, 2005) with the primers 5′-acgacctcgagggtggcggtggcggtatgtctaaaggtgaagaattattcgg-3′ and 5′- gacgacgcggccgcttatttgtacaattcatccataccatg-3′. YPet cDNA was amplified from pBAD33-YPet-His (Addgene plasmid #14031) (Nguyen and Daugherty, 2005) with the primers 5′-gacgacctcgagggtggcggtggcggtatgtctaaaggtgaagaattattcactgg-3′ and 5′- gacgacgcggccgcttatttgtacaattcattcataccctcg-3′. The resulting PCR fragments were cloned into the plasmids pGEX-6P1 using the EcoRI/XhoI/NotI restriction sites to obtain plasmids pGEX-6P1-HTTEx1Q48-CyPet and -YPet, respectively. To generate the plasmids encoding GST-Ex1Q23-CyPet and -YPet or GST-Ex1Q23 the coding sequence of HTTEx1Q23 was PCR-amplified from pDONR221-HTTEx1Q23 using the primers 5′-gac gacgaattcatggcgaccctg-3′ and 5′-gacgacgcggccgcctcgagtggtcggtgcagcgg-3′ (GST-Ex1Q23-CyPet and -YPet) or 5′-gacgac gaattcatggcgaccctg −3′ and 5′-gacgacgcggccgcctcgagttatggtcggtgcagcgg-3′. The resulting PCR products were digested using EcoRI and XhoI endonucleases and cloned into the plasmids pGEX-6P1-HTTEx1Q48-CyPet, -YPet or pGEX-6P1-HTTEx1Q48 after excision of HTTEx1Q48 fragments by EcoRI/XhoI endonucleases.

Recombinant protein expression

The proteins GST-Ex1Q23, -Ex1Q48, -Ex1Q23-CyPet, -Ex1Q23-YPet, -Ex1Q48-CyPet and -Ex1Q48-YPet were produced in *E. coli* BL21-CodonPlus-RP and affinity-purified on glutathione-Sepharose beads. Purified proteins were dialyzed over night at 4°C against 50 mM Tris-HCl pH 7.4, 150 mM NaCl, 1 mM EDTA and 5% glycerol, snap-frozen in liquid N_2 and stored at −80°C. Protein concentrations were determined with a NanoDrop spectrophotometer. Prior to use, protein solutions were ultra-centrifuged at 190,000 x g for 40 min to remove aggregated material. α-Synuclein (α-Syn) was produced in *E. coli* BL21 (DE3) and monomeric α-Syn was purified as described elsewhere (Theillet et al., 2016). Expression of Tau40 protein was performed in *E. coli* BL21 using a 50 l bioreactor. After cell disruption using a French press, Tau40 protein was purified via cation exchange chromatography and gel filtration. Expression and purification of Tau were performed by InVivo BioTech Services (Hennigsdorf, Germany) using proprietary company protocols.

Preparation of *in vitro* seeds

Spontaneous Ex1Q48 aggregation was initiated by addition of 14 U PreScission protease (GE Healthcare) per nmol purified GST-Ex1Q48 fusion protein (2 μM). The aggregation reaction was performed in 50 mM Tris-HCl pH 7.4, 150 mM NaCl, 1 mM EDTA and 1 mM DTT at 25°C and constant agitation (450 rpm) for 24 h. Ex1Q23 protein for seeding experiments was prepared from GST-Ex1Q23 fusion protein using the same protocol. Synthetic human IAPP was aggregated as described previously (Gao et al., 2015). Lyophilized α-Syn was dissolved in PBS at 500 μM and centrifuged (4°C, 265.000 x g) after a 5 min sonication step to remove aggregated material. The supernatant was incubated for 7 d at 37°C under constant shaking in the presence of a single glass bead. Tau40 was aggregated for 6 d at 37°C under constant shaking in 100 mM sodium acetate, pH 7.4, and 1 mM DTT in the presence of heparin. Synthetic human $A\beta_{1-42}$ was dissolved in 100 mM NaOH and diluted to 200 μM in low salt buffer (10 mM K_3PO_4, pH 7.4, 10 mM NaCl). Aggregation was performed for 6 h at 37°C under constant agitation.

Atomic force microscopy

Aliquots of 15 μl aggregation reactions (24 h) were spotted onto freshly cleaved mica glued to a microscope slide. After incubation for 30 min to allow adsorption, samples were rinsed 4 times with 40 μl distilled water and dried over night at RT. Samples were imaged with a digital multimode Nanowizard II (JPK, Germany) atomic force microscope operating in intermittent-contact mode.

Filter retardation assays

FRAs were essentially performed as described previously (Wanker et al., 1999). Briefly, equal volumes of 500 ng of Ex1Q48 aggregates and 4% SDS solution with 100 mM DTT were mixed and boiled at 95°C for 5 min. By applying vacuum, samples were filtered through a cellulose acetate membrane with 0.2 μm pores (Schleicher and Schuell, Germany) and washed twice with 100 μl 0.1% SDS. For analysis of tissue homogenates, 60 μg of total protein for mouse brain and 75 μg of total protein for *Drosophila* heads were filtered per dot. Membranes were blocked with 5% skim milk in PBS/0.05% Tween20 (PBS-T) for at least 30 min. Aggregates retained on the membrane were detected using GFP, N18, MW8, MAB5492 or HD1 antibody followed by an appropriate peroxidase-coupled secondary antibody. Signals were quantified using the AIDA image analysis software (Raytest, Germany).

Dot blot assays

To estimate total HTT protein, native dot blot (DB) assays were performed as described previously (Kayed et al., 2003). Briefly, 250 ng of Ex1Q48 protein were filtered onto a nitrocellulose membrane and blocked with 5% skim milk in PBS-T. For detection, the membrane was incubated with HD1 antibody followed by an appropriate peroxidase-coupled secondary antibody. Signals were quantified using the AIDA image analysis software (Raytest, Germany).

Native gels

Protein solutions were mixed with sample buffer and loaded onto a Novex NativePAGE 3%–12% Bis-Tris gradient gel (Life Technologies). NativePAGE and immunoblotting were performed according to manufacturer recommendations. Ex1Q48 aggregates were visualized as for SDS-PAGE.

SDS-PAGE and Western blotting

Samples of aggregation reactions were mixed with loading buffer (50 mM Tris-HCl pH 6.8, 2% SDS, 10% glycerol and 0.1% bromophenol blue) and boiled at 95°C for 5 min. Samples were loaded onto Novex NuPAGE 4%–12% Bis-Tris gradient gels (Life Technologies). SDS-PAGE and immunoblotting were performed according to manufacturer recommendations. Ex1Q48 distribution was visualized by N18 antibody (Santa Cruz) or Ex1Q48-CyPet/-YPet with a GFP antibody (Abcam) followed by appropriate peroxidase labeled secondary antibodies.

Genotyping of *Drosophila* strains

Total genomic DNA from transgenic flies was extracted using the DNeasy® Blood & Tissue Kit (QIAGEN). cDNAs encoding HTTex1Q17 and HTTex1Q97 were PCR amplified using the Pwo DNA polymerase (Roche) and the primers 5′-aaccccgtaaatcaactgc- 3′ and 5′-atctctgtaggtagtttgtc-3′). The sizes of the resulting PCR products were analyzed by agarose gel electrophoresis.

Quantitative polymerase chain reaction (qPCR)

RNA was extracted from *Drosophila* heads using TRIzol Reagent (Invitrogen). cDNA was synthesized using M-MLV Reverse Transcriptase (Thermo Scientific) and qPCR was performed using the SYBR Green PCR Master Mix (Thermo Scientific). Primer pairs for HTT (sense, 5′-gacctggaaaagctgatga-3′ and antisense 5′-tcatggtcggtgcagcggct-3′), and control primers for rp49 (sense 5′-ta caggcccaagatcgtgaa-3′, and antisense 5′-acgttgtgcaccaggaactt-3′) were utilized. SYBR Green analysis was performed using the ViiA7 Real-time PCR system (Thermo Scientific). The amount of mRNA detected was normalized to control rp49 mRNA values.

Viability analysis of adult *Drosophila melanogaster*

Viability assays were performed with elavGS;HTTex1Q17, elavGS;HTTex1Q97 and elavGS;HSPA1L;HTTex1Q97 transgenic flies by quantification of lethality of at least 100 females of each genotype and expression condition in three independent biological

replicates. Flies were aged at 25°C, with 10 flies per vial and were transferred every 3-4 days. Median lifespan (age at which half of the tested population has died) was calculated by fitting survival curves to the log(inhibitor) versus normalized response (variable slope) equation using GraphPad Prism. Statistical significance was assessed by one-way ANOVA followed by Dunnett's multiple comparison post hoc test. *, $p \leq 0.05$; **, $p \leq 0.01$; ***, $p \leq 0.001$.

Analysis of motor performance (climbing assay)

Ten female flies were placed in a closed empty vial and gently tapped to the bottom of the vial. The percentage of flies that climbed 8 cm within 15 s was recorded. Flies were aged at 25°C (10 flies per vial) and were monitored and transferred twice a week. Motor performance was assessed for elavGS;HTTex1Q17 and elavGS;HTTex1Q97 flies expressing the HTT transgenes for the indicated times. 100 females of each genotype and expression condition in each of the three biological replicates were investigated.

Preparation of *Drosophila* head lysates for FRAs

Drosophila head lysates were produced by homogenizing fly heads in 2% SDS and complete protease inhibitor cocktail using a micro pestle. Lysates were centrifuged for 10 min at 8,000 rpm (4°C). The supernatant was transferred to a new tube and total protein concentration was determined with a Pierce BCA assay using BSA as a standard.

Dissection and immunostaining of *Drosophila* adult brain

The whole brains of adult flies were dissected in ice-cold haemolymph-like saline (HL3) solution (Stewart et al., 1994), fixed for 20 min in 4% paraformaldehyde (PFA) in PBS and permeabilized in PBS-T (1% Triton™ X-100) for 20 min at RT. Samples were blocked in 10% normal goat serum (NGS) in PBS-T (0.3% Triton™ X-100) for at least two hours. Brains were incubated with the indicated primary antibody (1:500) in brain staining buffer (5% NGS, 0.1% NaN_3 in PBS-T (0.3% Triton™ X-100)) for 48 hours at 4°C. Subsequently, brains were washed in PBS-T (0.3% Triton™ X-100) for 24 hours at 4°C with multiple buffer exchanges. Next, samples were incubated with appropriate secondary antibody in brain staining buffer for 24 hours at 4°C, washed six times for 30 min in PBS-T (0.3% Triton™ X-100) at RT and stored in VectaShield H-100 (Vector Laboratories) at least for one day at −20°C. Brains were mounted and imaged using the Leica TCS SP8 Confocal Microscope. Images were analyzed using Fiji.

RNA interference

For synchronization, gravid adults from one 10 cm NGM plate were collected in a canonical tube and treated with 20% alkaline hypochlorite solution under vigorous agitation for 4 min. The eggs were then washed three times with cold 0.1 M NaCl solution. The eggs were allowed to hatch in M9 medium at 20°C for 22 h. Animals were then placed as L1 larvae onto RNAi plates that were seeded with *E. coli* expressing dsRNAi against *hsp-1* or the empty vector L4440 (control).

Fluorescence microscopy

The aggregation propensities of Q35-YFP were analyzed throughout adulthood. Animals were subjected to RNAi treatment from the first larval stage on and maintained on RNAi plates throughout the experiment. For imaging, nematodes were mounted onto 2% agarose (Sigma) pads on glass slides and immobilized with 2 mM Levamisole (Sigma). Images were taken on a Zeiss LSM780 confocal microscope at 20x magnification. The Q35-YFP expressing nematodes were analyzed as whole nematode for quantification of the aggregates and an image was taken of the head region of every animal. 20 animals were analyzed for each condition.

Motility assay

Nematodes were transferred from liquid culture onto a blank (unseeded) NGM plate and allowed to acclimate for 15 min. The movement of the animals was digitally recorded at 20°C using a Leica M165FC microscope with a DFC3000G digital camera and the Leica LASX Software. Movies of 10 s were captured at 10 frames/s. Animals that crossed each other or those that escaped from the field of view were excluded from analysis. 20 animals were analyzed for each condition. Captured frames were merged into *.avi format, imported into Fiji (Schindelin et al., 2012) and analyzed using the wrMTrck plugin (http://www.phage.dk/plugins). The average speed of each animal was calculated by dividing its body length by the duration of each track (body length per second).

Tissue homogenization

Frozen brain tissue was cut on dry ice, weighed and homogenized in a 10-fold excess (w/v) of ice-cold 10 mM Tris-HCl pH 7.4, 0.8 M NaCl, 1 mM EDTA, 10% sucrose, 0.25 U/μl benzonase and complete protease inhibitor cocktail with a dounce homogenizer. The homogenate was incubated for 1 h at 4°C on a rotating wheel and centrifuged for 20 min at 2,700 x g (4°C) to remove cell debris. *Drosophila* heads were processed comparably using 10 μl of ice-cold 10 mM Tris-HCl pH 7.4, 0.8 M NaCl, 1 mM EDTA, 10% sucrose and a complete protease inhibitor cocktail per fly head. Homogenates were centrifuged for 10 min at 8,000 rpm (4°C). After centrifugation, supernatants were transferred to a new tube and total protein concentration was determined with a Pierce BCA assay using BSA as a standard. For FRASE analysis, 0.8-5 μg total protein per replicate were applied.

Electron microscopy

Total brain homogenate was centrifuged at 18,000 x g at 4°C for 20 min; the resulting supernatant was pelleted by ultra-centrifugation at 190,000 x g for 40 min and resuspended in 10 mM Tris-HCl (pH 7.4). Immunolabeling was performed with minor modifications as described (Laue, 2010). Briefly, samples were incubated on formvar-coated copper grids (Plano) for 10 min before immunolabeling. Grids were blocked and washed in PBS supplemented with 1% BSA and 0.1% glycine. Labeling was performed with the anti-HTT aggregate antibody Agg53 and an appropriate 12 nm colloidal gold-labeled secondary antibody (Jackson ImmunoResearch). Samples were stained with 2% uranyl acetate and imaged with a Zeiss EM 910 transmission electron microscope at 80 kV. Acquisition was performed with a CDD camera (Quemesa, Olympus Viewing System).

Immunodepletion of HTTex1 aggregates from mouse brain extracts

Protein G-coupled magnetic beads (Life Technologies) were incubated with 4 μg MW8 (Developmental Studies Hybridoma Bank, DSHB) or IgG isotype control (Invitrogen) antibody, respectively, for 10 min at RT to allow antibody binding. Free binding sites were saturated with Pierce protein-free blocking solution according to manufacturer recommendations. 500 μg brain homogenate in brain lysis buffer were incubated with antibody coupled beads for 3 h at 4°C under constant overhead rotation. Subsequently, aliquots from the supernatants were taken and analyzed with the FRASE assay.

FRASE assay

Purified GST-Ex1Q48-CyPet and GST-Ex1Q48-YPet were diluted in aggregation buffer at an equimolar ratio to a final concentration of 1.2 μM (0.6 μM each) with 14 U PSP per nmol sensor proteins if not stated otherwise. The solution was then mixed with preformed aggregates of Ex1Q48 (seeds) at varying concentrations with or without prior sonication and transferred to a black 384-well plate (with a final reaction volume of 30 μl per well and a sensor protein concentration of 1.2 μM). For quantification of seeding-competent HTT species in tissue samples, the sensor-protein mixture was supplemented with up to 10% (v/v) tissue homogenate. Fluorescence signals were measured every 20 min following a 5 s pulse of vertical shaking with a Tecan M200 fluorescence plate reader at 25°C for up to 48 h. CyPet donor fluorescence was measured at excitation (Ex): 435 nm/emission (Em): 475 nm; YPet acceptor fluorescence at Ex: 500 nm/Em: 530 nm; the FRET channel (DA) was recorded at Ex: 435 nm/Em: 530 nm. Raw signals were processed by subtracting the background fluorescence of unlabeled Ex1Q48 in all channels. Signals in the FRET channel were corrected for donor bleed-through (c_D) and acceptor cross excitation (c_A) using donor- and acceptor-only samples to obtain sensitized emission. Finally, sensitized emission was normalized to the acceptor signals (Jiang and Sorkin, 2002). In brief, the FRET efficiency E (in %) was calculated as follows: $E = (DA\text{-}c_D xDD\text{-}c_A xAA)/AA$ with DD = donor channel signal and AA = acceptor channel signal.

Quantification of mHTT seeding activity (HSA)

Seeding effects (Δt_{50} [h]) were quantified by subtracting the t_{50} values (time at half-maximal FRET efficiency) of the respective sample from the negative control. To obtain the t_{50} values, the aggregation kinetics were curve fitted by Richard's five-parameter dose-response curve using GraphPad Prism.

$$y = y_0 + \left(\frac{y_\infty - y_0}{\left(1 + 10^{((Logxb - x) \times HillSlope)}\right)^S} \right)$$

QUANTIFICATION AND STATISTICAL ANALYSIS

Statistical parameters including the exact value of n, the definition of center, dispersion and precision measures (mean ± SEM or mean ± SD) as well as the statistical analysis chosen and statistical significance are reported in the figures and figure legends. Data is judged to be statistically significant when $p < 0.05$ by the indicated statistical test. In figures, asterisks denote statistical significance (*, $p < 0.05$; **, $p < 0.01$; ***, $p < 0.001$). Statistical analysis was performed in GraphPad PRISM 7.